Wintertime Cold-Air Pools in the Bavarian Danube Valley Basin: Data Analysis and Idealized Numerical Simulations

GÜNTHER ZÄNGL

Meteorologisches Institut der Universität München, Munich, Germany

(Manuscript received 21 February 2005, in final form 24 June 2005)

ABSTRACT

This paper investigates wintertime cold-air pools in a basinlike part of the Danube Valley, located in the German state of Bavaria. Specifically, the focus is on cold-pool events restricted to the basin area, that is, not extending to the more elevated parts of the Alpine foreland. An analysis of observational data indicates that the delay of warm-air advection in the basin area relative to the Alpine foreland plays a major role in these events. However, the relationship between warming in the Alpine foreland and a temperature deficit in the northeast–southwest-oriented basin appears to depend sensitively on the ambient wind direction. A statistically significant correlation is found only for westerly and southerly wind directions but not for easterly directions. To examine the dynamical reasons for this phenomenon, idealized numerical simulations have been conducted. They are initialized with a pronounced cold pool in the basin area and examine the response of the cold pool to the dynamical forcing imposed by a geostrophically balanced large-scale wind field of various directions and strengths. Sensitivity tests consider the effects of the surrounding mountain ranges and of turbulent vertical mixing. The model results indicate that the most important dynamical processes capable of dissolving cold-air pools in a large basin are (i) ageostrophic advection of the cold air toward lower ambient pressure and (ii) downstream advection by the ambient flow. The former might also be interpreted as an adjustment of the cold air to the external pressure gradient, which can be balanced by the development of a spatial gradient in cold-pool depth. In principle, both advection processes are most effective in the along-basin direction because the advected air does not have to surmount significant topographic obstacles. However, a combination of several effects induced by the surrounding mountain ranges—for example, upstream flow deceleration and wake formation—modifies the dependence of the cold-pool persistence on the ambient wind direction. In agreement with observational data, the simulations with full topography predict a higher tendency for cold-pool persistence in the Danube basin for westerly and southerly flow than for easterly flow. Turbulent vertical mixing is found to make a significant contribution to the erosion of cold pools, but its effect is smaller than the sensitivity to the ambient wind direction.

1. Introduction

At mid- and high latitudes, wintertime high pressure situations are frequently associated with persistent cold-air pools, usually defined as a surface-based layer of high static stability that is not dissolved during the daytime heating period. Cold-air pools tend to be particularly long lived in valleys and basins, where the surrounding topography reduces the advective airmass exchange with the environment. In industrialized areas, they can lead to severe air pollution problems (e.g., Petkovšek 1985; Petkovšek and Vrhovec 1994) and, when associated with fog or low stratus, cause annoying and expensive delays to air traffic. Even worse traffic obstructions may occur because of freezing rain, which often accompanies wintertime warm front passages when cold-air pools keep the low-level temperature below freezing while positive temperatures prevail above.

Of the existing literature on cold pools, a large fraction focuses on radiative formation and destruction processes, starting with Whiteman (1982) and Whiteman and McKee (1982). These authors developed and validated a simple thermodynamical model for radiatively driven inversion breakup in valleys, based on an energy budget calculation for a specified valley geometry. Later on, numerical simulations were used to study, for example, the radiatively driven formation of a cold pool in an idealized basin (Vrhovec 1991) or in a

Corresponding author address: Dr. Günther Zängl, Meteorologisches Institut der Universität München, Theresienstraße 37, D-80333 München, Germany.
E-mail: guenther@meteo.physik.uni-muenchen.de

real one having only one major outflow to the environment (Fast et al. 1996). Of course, observational studies on the formation of nocturnal cold-air pools in basins have been conducted as well (e.g., Whiteman et al. 1999a,b). Recently, Colette et al. (2003) investigated the cold-pool evolution in a steep mountain valley, pointing out the effect of topographic shading on the heat budget. However, most of the studies considering radiative processes have in common that the cold pools under investigation do not persist throughout the daytime heating period. An exception is the paper by Vrhovec and Hrabar (1996), who examined a situation in which snow cover kept the daytime solar heating small.

Another significant fraction of the previous literature investigates dynamical mechanisms capable of destroying a cold-air pool, with some emphasis on turbulent vertical mixing. Studying the interaction between gravity wave–driven downslope winds and a leeside cold pool, Lee et al. (1989) found that turbulent mixing is usually not effective enough to erode the cold pool. The formation of a large-amplitude gravity wave penetrating down the lee slope was obtained only if a pressure gradient favorable for the downstream advection of the cold pool was imposed. However, Vrhovec and Hrabar (1996) reported that turbulent mixing related to ambient winds could break up the cold pool in a snow-covered basin in conjunction with solar heating, while the heating alone is too weak to remove the cold air. Several other studies (e.g., Petkovšek 1992; Rakovec et al. 2002; Zhong et al. 2003) pointed out that the ambient winds have to be really strong ($\sim$20 m s^{-1} or more) to effectively erode a cold pool by turbulent mixing alone. For large basins, such as the Danube basin investigated in this study, Petkovšek and Vrhovec (1994) found that the redistribution of the cold air mass resulting from a horizontal pressure gradient imposed on top of the cold pool (e.g., related to a geostrophically balanced ambient flow) might be more important than vertical mixing for light to moderate wind speeds. Because the cold air tends to accumulate on that side of a basin where the ambient pressure is low, part of a basin might get out of the cold pool without the need of any turbulent mixing or radiative heating (see also Zängl 2003a). On the other hand, drainage flows can substantially reduce the stability of cold pools in deep mountain valleys (Zängl 2003a). Moreover, Zhong et al. (2001) noted that cold-air advection aloft can be an important factor leading to the disappearance of a cold pool, if other erosion processes are not effective enough. They also pointed out that warm-air advection at higher levels, related to horizontal advection and/or to subsidence, is an important formation or strengthening process for cold pools in cases of preexisting cold air.

The primary limitation of most previous studies on dynamical processes affecting cold-air pools, with the exception of Zhong et al. (2001), is their restriction to highly idealized topography configurations. While considering idealized topography is an important starting point for studying processes, more realistic settings need to be investigated as well in order to estimate the practical importance of the processes identified in the idealized studies. In the present work, we would like to make one step in this direction, examining several dynamical aspects of cold-air pools in the basin-like part of the Danube Valley in the German state of Bavaria (see Fig. 2 for location). This basin is located 70–150 km north of the Alpine baseline and is bordered to its northeast by a mountain range called the Bavarian/Bohemian Forest, implying that there could be a substantial impact of the surrounding topography on the cold-pool behavior in the basin. The simulations conducted to investigate the cold-air pools in the Danube basin are still idealized in the sense that they are not initialized with real atmospheric data, but they consider realistic topography and a wide range of typical large-scale flow conditions. They include sensitivity experiments with modified topography designed to elucidate the impacts of the Alps and the Bavarian/Bohemian Forest, and tests with suppressed vertical temperature mixing to directly reveal its impact on cold-pool erosion. Moreover, the simulations are complemented by a statistical analysis to demonstrate the basic characteristics of observed cold-air pools. The main reason for not considering a specific case (as had originally been planned) is that the density of the operational weather stations is insufficient for a meaningful case study. In particular, there is no radiosonde station in the basin region.

The remainder of this paper is organized as follows. The data analysis and the goals of this study are presented in section 2. Section 3 describes the setup of the numerical experiments. Section 4 presents the results, which are applied to the observational data in section 5. The main conclusions are summarized in section 6.

2. Data analysis

In central Europe, one of the regions exhibiting a marked local maximum in the persistence of cold-air pools is the basin-like part of the Danube Valley in eastern Bavaria. Although it is not rare for persistent cold-air pools to cover the whole northern Alpine foreland, there are many cases in which the cold-air pool is restricted to the Danube basin, or at least is substantially more pronounced than at higher elevations. In the

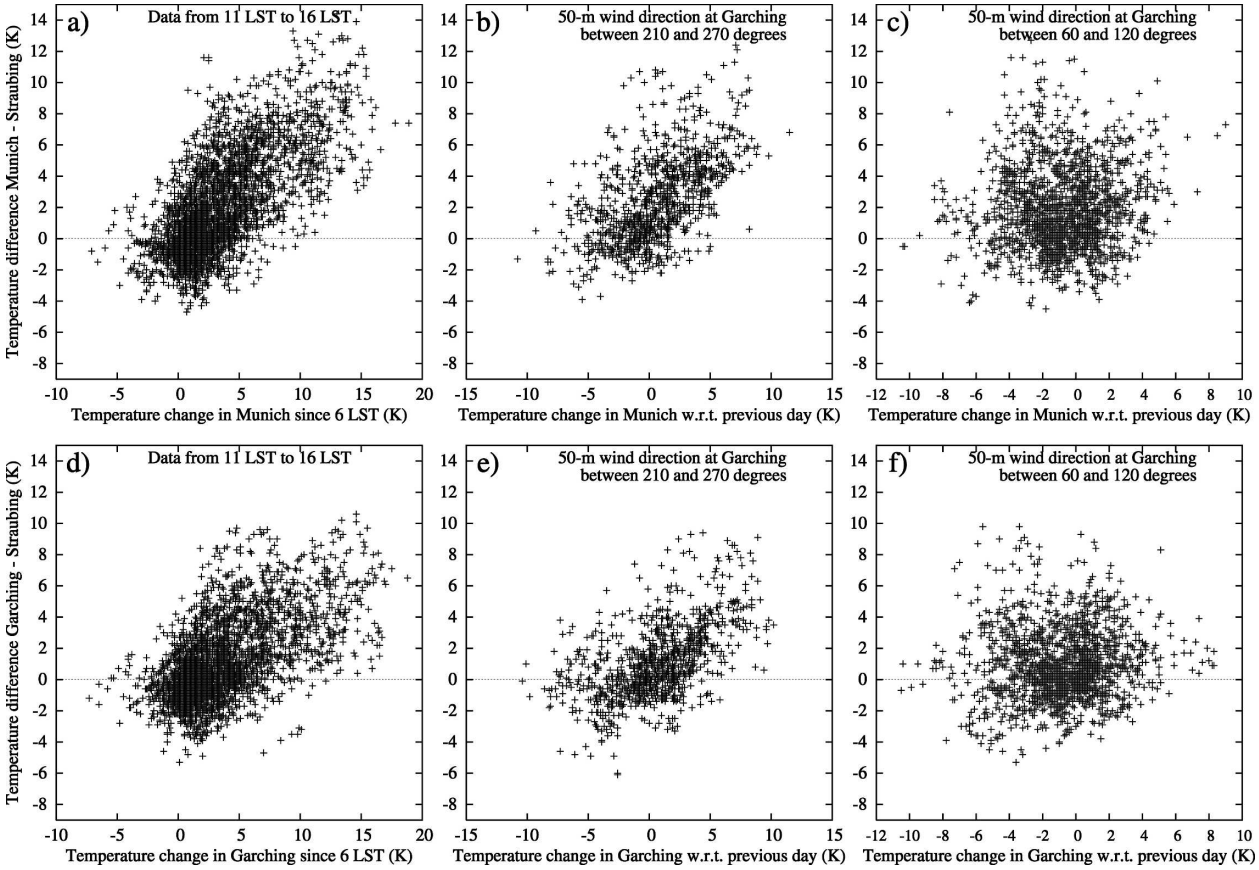

FIG. 1. Scatterplots showing the relationship between a temperature change in (top) Munich or (bottom) Garching and the temperature difference between Munich/Garching and Straubing.

following, we want to focus on the latter type of cold-air pools and briefly illustrate the basic characteristics and the climatological relevance of these events.

From synoptic experience, it is known that many of these cold-pool events occur under the influence of an extended high pressure system, with large-scale subsidence causing high temperatures and low humidity in the free atmosphere. In such situations, the nocturnal surface inversion tends to be dissolved during the day at higher elevations (particularly in the absence of a continuous snow cover), whereas the cold pool persists in the basin. One important contribution to these differences arises from the larger cold-pool depth in the basin area, which implies that a larger heat input is needed to break up the surface inversion (see e.g., Whiteman and McKee 1982). Moreover, haze or low stratus clouds often reduce the solar heating in the basin area. An illustration of this effect is given in Figs. 1a,d, showing scatterplots relating the temperature spread between the basin and its surroundings to the daytime heating outside the basin. Specifically, the 2-m temperature difference between Munich and Straubing (Fig. 1a) and between Garching and Straubing (Fig. 1d, see Fig. 2b for the location of the stations) is displayed against the temperature increase since 0600 local standard time (LST) at Munich and Garching, respectively. Because Straubing is the basin station, a positive value on the *y* axis corresponds to a temperature deficit within the basin. The database used for this analysis is hourly temperature data for the years of 1995–99, restricted to the months of November through February. Moreover, data points are restricted to times between 1100 and 1600 LST in Figs. 1a,d so as to focus on temperature changes related to the diurnal cycle. From the results, it is obvious that a strong daytime heating in the region of Munich is correlated with temperature excess relative to the Danube basin, where the diurnal temperature amplitude tends to be substantially lower in the winter months. The correlation coefficient is 0.70 (0.60) for the station pair of Munich–Straubing (Garching–Straubing). The differences between Munich and Garching mainly arise from the fact that the station in the city of Munich is affected by a pronounced urban heat island effect while Garching is not.

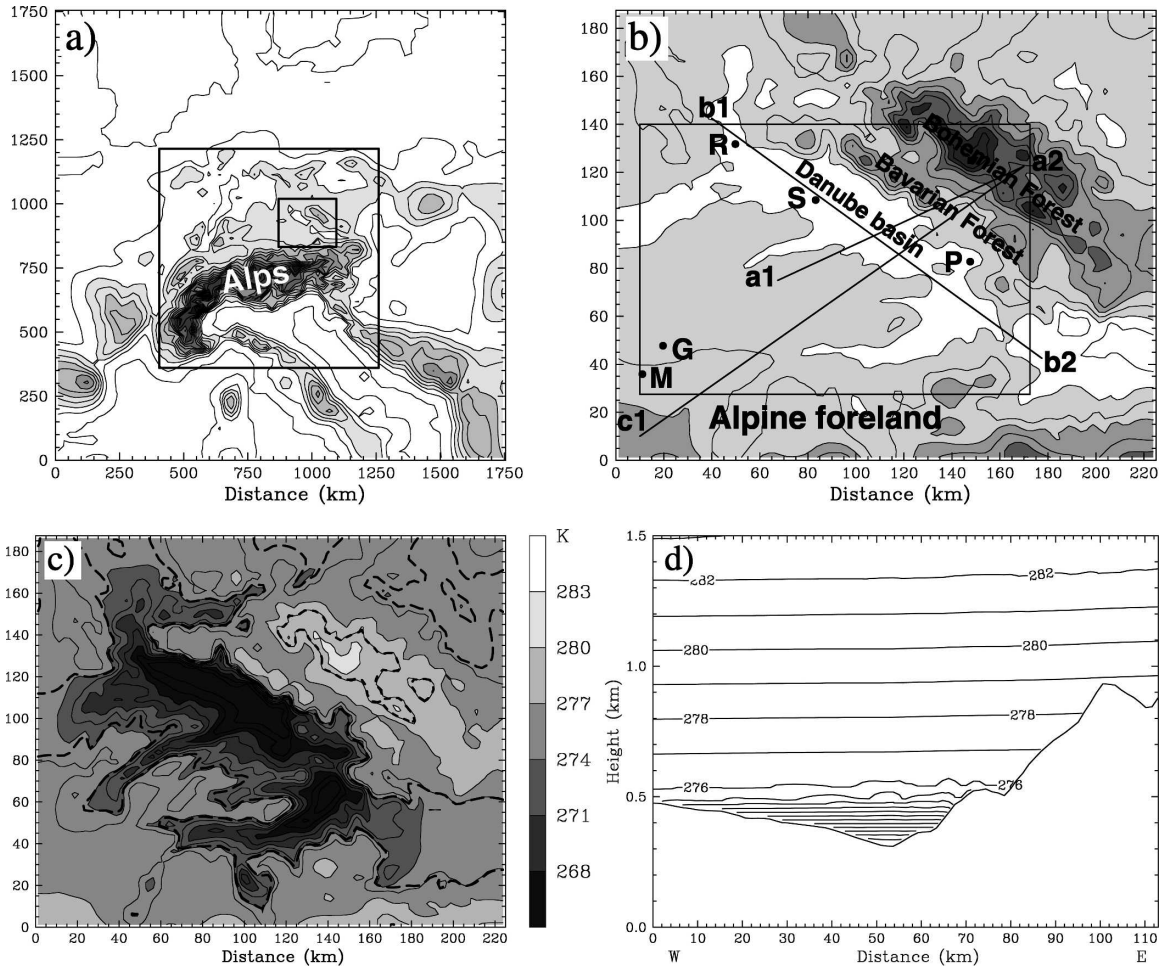

FIG. 2. (top) Model topography in the (a) second domain and (b) fourth domain. In (a), the contour interval and the shading increment are 200 and 400 m, respectively, and the boxes indicate the location of the nested model domains. In (b), the contour interval (shading increment) is 100 m (200 m), with no shading below 400 m. Locations are Munich (M), Garching (G), Regensburg (R), Straubing (S), and Passau (P). Solid lines indicate the positions of vertical cross sections shown later in this paper, and the box marks a subdomain used for further analysis. (bottom) Initial potential temperature field (c) at surface level and (d) along cross section a1–a2. Contour intervals are 1.5 K in (c) and 1 K in (d). The shading increment in (c) is 3 K, and long (short)-dashed contours indicate a topography height of 450 (900) m.

The other type of synoptic condition that is favorable for pronounced temperature differences between the Danube basin and the surrounding areas is warm-air advection. Relative to the more elevated regions of the Alpine foreland, the penetration of the warm air to the ground tends to be delayed in the basin, forming a localized cold pool typically lasting for between 12 and 24 h. An important practical consequence of this delay is that freezing rain is much more frequent in the Danube basin than, for example, in the region of Munich. To illustrate the relationship between warm-air advection and the presence of a cold pool in the Danube basin, we present scatterplots between the Munich–Straubing (Garching–Straubing) 2-m temperature difference and the temperature change at Munich (Garching) during the preceding 24 h. Data are now used from all hours of the day but are separated into different groups according to the 50-m wind direction measured at Garching, where a meteorological tower is located. Results are shown in Fig. 1 for the range of 210°–270° (Figs. 1b,e) and for the range of 60°–120° (Figs. 1c,f). In both cases, the 50-m wind speed is required to range between 2 and 8 $m\,s^{-1}$, and the wind direction is required to stay within the same interval for at least 4 h. Some basic statistical quantities are summarized in Table 1, including the other directional ranges not shown in Fig. 1.

For advective warming from the west or southwest (210°–270°), there is a significant correlation between the basin–environment temperature difference and the advective warming outside the basin (Figs. 1b,e). The

TABLE 1. Summary of the statistical data analysis. Abbreviated station names are Garching: Gar, Straubing: Str, Munich: Mun, Regensburg: Reg, and Passau: Pas (see Fig. 2b for location). The correlation coefficient is defined as $[\Sigma(T_{1_i} - \overline{T_1})(T_{2_i} - \overline{T_2})]/\{[\Sigma(T_{1_i} - \overline{T_1})^2\Sigma(T_{2_i} - \overline{T_2})^2]^{1/2}\}$, where T denotes temperature and the indices 1 and 2 represent a station pair. The index i indicates the summation, and an overbar denotes the average value.

Stations	Wind direction	No. of data	Mean difference	Correlation coeff
Gar–Str	60°–120°	1699	0.92 K	0.06
Gar–Str	120°–210°	890	0.71 K	0.52
Gar–Str	210°–270°	973	1.11 K	0.55
Gar–Str	270°–330°	1410	0.15 K	0.43
Gar–Str	330°–60°	347	−0.40 K	0.30
Mun–Str	60°–120°	1714	1.82 K	0.07
Mun–Str	210°–270°	973	2.45 K	0.55
Mun–Str	330°–60°	356	−0.05 K	0.22
Gar–Reg	60°–120°	1670	0.25 K	0.10
Gar–Reg	210°–270°	971	0.53 K	0.59
Gar–Reg	330°–60°	347	−0.18 K	0.18
Gar–Pas	60°–120°	972	0.05 K	0.14
Gar–Pas	210°–270°	210	1.47 K	0.69
Gar–Pas	330°–60°	140	−0.23 K	0.42

corresponding correlation coefficient is 0.55 in both cases (Table 1). On the other hand, the correlation coefficient is almost zero (0.06 and 0.07) for wind directions between 60° and 120° (Figs. 1c,f). Table 1 also shows that similar correlation coefficients are obtained for Regensburg, which is located in the northwestern part of the basin (see Fig. 2b). The station of Passau exhibits generally higher correlation coefficients, but it has to be noted that the data availability is restricted to the years of 1995 and 1996 for Passau because the station was moved uphill afterward. Restricting the statistical evaluation of the other stations to these years also leads to higher correlation coefficients, though remaining somewhat lower than for Passau.

The remaining wind direction classes are found to range in between these extreme cases. For wind directions between 120° and 210°, the correlation exceeds again 0.5, whereas it ranges between 0.4 and 0.45 for the interval of 270°–330°. The correlation coefficients found for Regensburg and Passau are similar to those for Straubing in these cases (not shown). A special situation is encountered for northerly/northeasterly flow (330°–60°). Because of the flow deflection induced by the Alps, winds from this sector do not tend to remain stationary for a long time in the Alpine foreland, which shows up in Table 1 as a comparatively small number of available data. Moreover, there are substantial differences between the correlation coefficients for Regensburg, Straubing, and Passau, with the lowest values found at Regensburg and the highest ones at Passau. This implies that for northerly flow, the warming delay in the Danube Valley increases from northwest to southeast (see Fig. 2b).

In the remainder of this paper, we will focus primarily on investigating the reasons for the dependence of the warming delay in the Danube basin on the wind direction. This will be accomplished by idealized numerical simulations in which an initial cold pool in the Danube basin is exposed to ambient winds of various directions. Most of the simulations discussed in the following will disregard radiative effects so as to concentrate on dynamical effects. This is a meaningful simplification because warm front passages are often associated with overcast skies, implying that the net radiative forcing is small. Sensitivity experiments regarding the interaction between ambient wind speed and daytime radiative heating will also be presented, but a thorough investigation of fog and haze effects is left for a future study. Though qualitatively easy to understand, the effects of fog and haze are difficult to model because the physics parameterizations available in current mesoscale models are not sophisticated enough. For example, a proper representation of haze requires a separate prognostic variable for the aerosol concentration and a sophisticated radiation scheme accurately accounting for the interactions between aerosols, atmospheric humidity, and radiation. Likewise, most microphysical parameterizations have weaknesses in maintaining fog or low stratus clouds because of too rapid drizzle formation, which in turn is related to the lack of an aerosol variable for the condensation nuclei abundance.

3. Setup of the numerical experiments

The numerical simulations presented in this study have been conducted with the fifth-generation Pennsylvania State University–National Center for Atmospheric Research Mesoscale Model (MM5), version 3.3 (Grell et al. 1995). The model solves the nonhydrostatic equations of motion in a terrain-following sigma-coordinate system. Four interactively nested model domains are used with horizontal mesh sizes of 67.5, 22.5, 7.5, and 2.5 km, respectively. The corresponding numbers of grid points are 79×73, 79×79, 115×115, and 91×76, respectively. The first domain is centered close to the Danube basin at 49°N, 11.5°E and covers a large part of Europe and the North African countries. The area covered by the second domain is displayed in Fig. 2a, together with the location of the two innermost domains, and a close-up view of the fourth domain is provided in Fig. 2b. The model topography was created from U.S. Geological Survey (USGS) digital elevation data with a resolution of 5′ (domains 1–2) and 30″ (do-

mains 3–4). For sensitivity experiments, this topography was artificially modified by cutting either the Alps at a height of 800 m or the Bavarian/Bohemian Forest at a height of 550 m. Information on land use categories was also obtained from USGS data with the same resolution as the terrain data. In the vertical, 39 full-sigma levels are used, corresponding to 38 half-sigma levels where all variables but the vertical wind are computed. The lowermost half-sigma level, which will be referred to as the surface level in the remainder of this paper, is located about 10 m above ground. The vertical spacing between the model layers ranges between 35 m near the surface and 750 m near the upper-model boundary, which is located at 100 hPa. At the upper boundary, an improved version of the Klemp and Durran (1983) radiation condition is used to prevent spurious reflections of vertically propagating gravity waves (see Zängl 2002a).

The majority of the simulations were conducted in a dry mode (no cloud microphysics) without consideration of radiation processes. Only a boundary layer parameterization is retained in these simulations in order to account for the effects of surface friction and turbulent vertical mixing. We use a 1.5-order closure scheme based on a predictive equation for turbulent kinetic energy (TKE) that was validated within the MM5 modeling system by Shafran et al. (2000). For sensitivity experiments, the vertical mixing of temperature is artificially switched off in order to examine its impact on the temperature evolution within the cold pool. It is noted that in these tests, the suppression of the vertical mixing is applied in the innermost model domain only because the low-level stratification of the ambient air mass would change otherwise, which might have undesired side effects on the flow dynamics. All simulations employ the modified scheme for horizontal numerical diffusion described by Zängl (2002b), in which the diffusion of temperature and the mixing ratios of water vapor and cloud water is computed truly horizontally rather than along the terrain-following coordinate surfaces. As demonstrated by Zängl (2003a), using this modified diffusion scheme is of crucial importance for a meaningful simulation of the evolution of cold-air pools. A recent study by Zängl (2005a) revealed that it even allows for a realistic simulation of cold-air pools in narrow Alpine valleys. Moreover, the generalized vertical coordinate described by Zängl (2003b) is used. It allows for a rapid decay with height of the topographic structures in the coordinate surfaces. The main advantage of this type of generalized coordinate is that horizontal advection over mountainous terrain becomes more accurate (see also Schär et al. 2002).

The large-scale wind field prescribed in the simulations is horizontally homogeneous and in geostrophic balance with the pressure field except for the frictional boundary layer. For consistency, the Coriolis parameter is set to a constant value of 10^{-4} s^{-1}. The wind field has positive shear but a constant direction (again except for the frictional boundary layer), which is varied from 45° through 360° at increments of 45° with a refinement to 22.5° for the climatologically most frequent directions between 225° and 315°. At the initial time, the large-scale wind speed is zero at sea level and increases linearly with height up to 12.5 m s^{-1} at tropopause level (250 hPa). During the first 12 h of the simulations, the sea level wind speed is accelerated to either 7.5 or 12.5 m s^{-1} through imposing a forcing at the lateral boundaries, which is transmitted to the domain of interest via geostrophic adjustment within a couple of hours. These wind speeds are chosen because they are within the climatological range of variability for all wind directions (Schipper 2005). The vertical shear is maintained during the acceleration procedure, implying that the final wind speed at tropopause level is 20 and 25 m s^{-1}, respectively. After $t = 12$ h, the forcing at the lateral boundaries remains constant until the termination of the simulations at a model time of 48 h. The initial temperature field in the model center starts with a sea level temperature of 273.15 K (0°C), followed by vertical gradients of -2.5 K km^{-1} below 850 hPa and -6.5 K km^{-1} between 850 and 250 hPa. Higher above, an isothermal stratosphere is assumed. Horizontal temperature gradients are specified according to thermal wind balance. In the Danube basin region, specifically in the box 48°–49°N, 12°–13.5°E, a cold pool is prescribed at the initial time by reducing the temperature below a height of 500 m MSL by 10 K over a depth of 175 m. The transition zone at the lateral edges of the box has a width of 0.5° latitude and 0.5° longitude. The resulting temperature field in the innermost model domain is displayed in Figs. 2c,d.

The sensitivity experiments with radiation use the so-called rapid radiative transfer model (RRTM) scheme (Mlawer et al. 1997) and also a simple cloud microphysics parameterization (Dudhia 1989), the usage of which is required by the RRTM scheme because it accounts for the interactions with moisture and clouds. The model date according to which radiation is computed is set to 15 November in these simulations, and the starting time is 1800 UTC. Again, the simulations are integrated over 48 h. The initial temperature field prescribed in these tests is specified in the same way as for the dry experiments except that the initial cold pool is omitted. Preliminary tests with an initial cold pool revealed that in the absence of fog, the cold pool is removed by radiative heating during the first

day of the simulation, implying that the initial condition is only of temporary relevance in this case. However, as discussed above, investigating the effects of fog is left for a future study because this probably requires more sophisticated parameterizations. To exclude the formation of fog everywhere in the model domain, the initial relative humidity is set to quite low values, ranging between 35% in the lower troposphere and 5% in the stratosphere.

4. Results

a. Weak-wind experiments

We start our discussion with the weak-wind simulations, that is, the simulations having a final sea level wind speed of 7.5 m s^{-1}. Model output time series describing the evolution of the cold pool in these experiments are shown in Fig. 3. The upper panels display the evolution of the area having a surface potential temperature below 273 K, normalized by the value at the initial time. Only model grid points lying within the rectangle indicated in Fig. 2b and having a topography height of less than 500 m MSL enter into this computation, roughly corresponding to the initial spatial extent of the cold pool. This implies that cold air that is advected out of the initial cold-pool area is not counted. We note in passing that the slight increase of the cold-pool area during the spin-up phase of the simulations (up to a factor of 1.18) is related to the fact that the initial cold pool is not in dynamical balance and therefore tends to spread out in the along-valley direction. This could have been avoided by extending the cold pool to the up- and downstream parts of the Danube Valley, but we wished to have a cold pool of limited extent to highlight the advection effects. Moreover, it is pointed out that the large-scale wind direction prescribed in the simulations does not necessarily match the local wind direction observed at Garching (see section 2) because the low-level flow field is strongly affected by the Alps. The application of the model results to the observations will be discussed in section 5b.

The results in Figs. 3a,b indicate that the cold pool is dissolved most rapidly for wind directions of 135° and 180°, followed by 360°. On the other hand, most of the initial cold pool persists for a direction of 45°, without any significant development during the second day of the simulation. For the westerly wind directions (225°–315°) and for easterly wind (90°), the cold pool is gradually eroded, and it is interesting to note that the variability among these simulations is smaller than the difference to either the 45° case or the 135° and 180° cases. For the westerly wind directions, the reduction of the cold-pool area during the first day of the simulation is faster for the cases with a northerly component (292° and 315°), but the results approach each other again on the second day.

Another way to look at the evolution of the cold pool is provided in Figs. 3c,d, showing the evolution of the minimum potential temperature $\theta_{\min}$ within the above-mentioned analysis area. This reveals, in addition, that the amount of temperature increase related to the erosion of the cold pool is somewhat smaller for southerly flow than for southeasterly and northerly flow. Moreover, the cold pool gets fully dissolved within the 48 h of simulation for 90° and 315°, while it does not for 225° through 292° despite a steady gradual increase of $\theta_{\min}$. For northeasterly flow, it is seen that the total increase of $\theta_{\min}$ is only slightly more than 2 K, again with little change during the second day of the simulation.

The difference between $\theta_{\min}$ and θ at the grid point closest to Garching is added in Figs. 3e,f in order to facilitate the subsequent application of the model results to the observations presented in section 2. Note that Garching lies within the analysis area, so that the temperature difference cannot become positive. Most notably, the result for 180° shows that the temperature difference between Garching and the coldest point remains between −5 and −7 K even after the disappearance of the cold pool proper. Moreover, the difference curve goes through a pronounced minimum of about −14 K at $t = 18$ h. This peak is related to subsidence of potentially warm air from the Alps (foehn), which happens to reach Garching shortly before the cold pool in the basin area is dissolved (see Fig. 4d below). Comparing Figs. 3c and 3f also reveals an interesting difference between easterly and westerly flow. Although the $\theta_{\min}$ values are close to each other until $t = 36$ h for 90° and 225° through 315°, the difference is several degrees smaller for 90° than for the westerly directions.

To illustrate the flow dynamics leading to these different temperature evolutions, Figs. 4 and 5 present surface fields of potential temperature, combined with the wind field at the third model level (about 85 m AGL). Taking the wind field from the third level was necessary for reasons of readability, because the wind at the lowermost model level (10 m AGL) is very weak in some of the experiments. Results are shown for $t =$ 24 h, except for the wind directions of 135°, 180°, and 360° (Figs. 4c,d and 5d), for which the results are displayed at $t = 18$ h, because the cold pool is fully eroded before $t = 24$ h. Selected vertical cross sections of wind and potential temperature are added in Fig. 6.

For northeasterly wind (Fig. 4a), a quasi-stationary wake forms in the lee of the Bavarian/Bohemian Forest mountain range (see Fig. 2b), which, for simplicity, will be referred to as the Bavarian Forest in the remainder

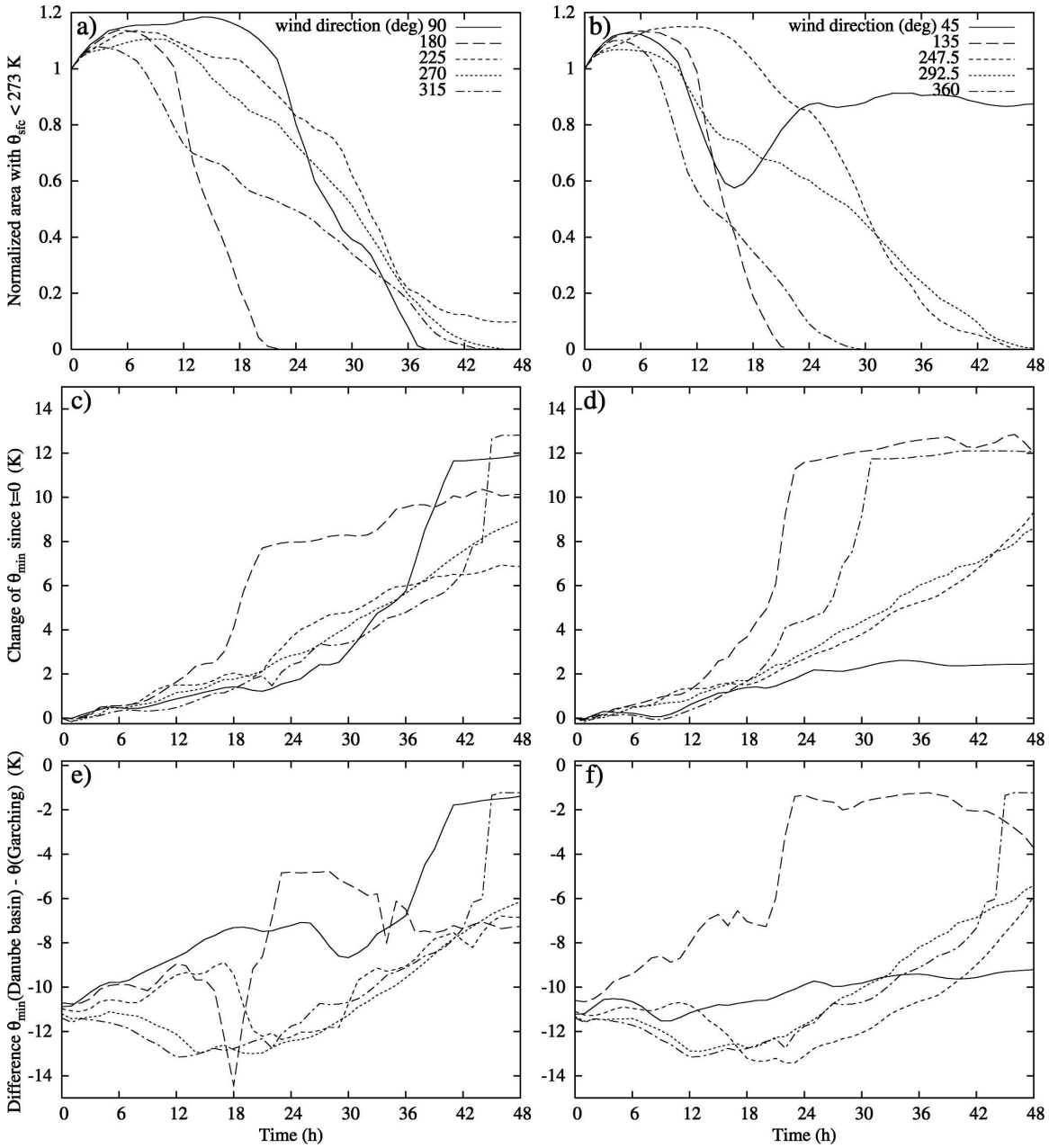

FIG. 3. Model output time series for the analysis area, defined as the intersection of the rectangle displayed in Fig. 2b with the 500-m-height isocontour. (top) Number of grid points having a surface potential temperature less than 273 K, normalized by its initial value. (middle) Change of the minimum potential temperature $\theta_{\min}$ in the analysis area since $t = 0$. (bottom) Difference between $\theta_{\min}$ and the surface potential temperature at Garching. The line key given in the upper panels is valid for all panels of the respective column.

of this paper. This wake formation is the primary reason for the longevity of the cold pool in the 45° case. Another important factor is the upstream flow deceleration induced by the Alps, which renders the low-level winds in the area under consideration generally quite weak. The impact of the Alps and the Bavarian Forest on the persistence of the cold pool will be examined in more detail in sections 4c and 4d, respectively.

At a wind direction of 90° (Fig. 4b), the Bavarian Forest still exerts a notable lee effect, but the angle between the orientation of the ridge line (about 310°–130°) and the ambient wind direction is smaller than for 45° and therefore is less optimal for the formation of a

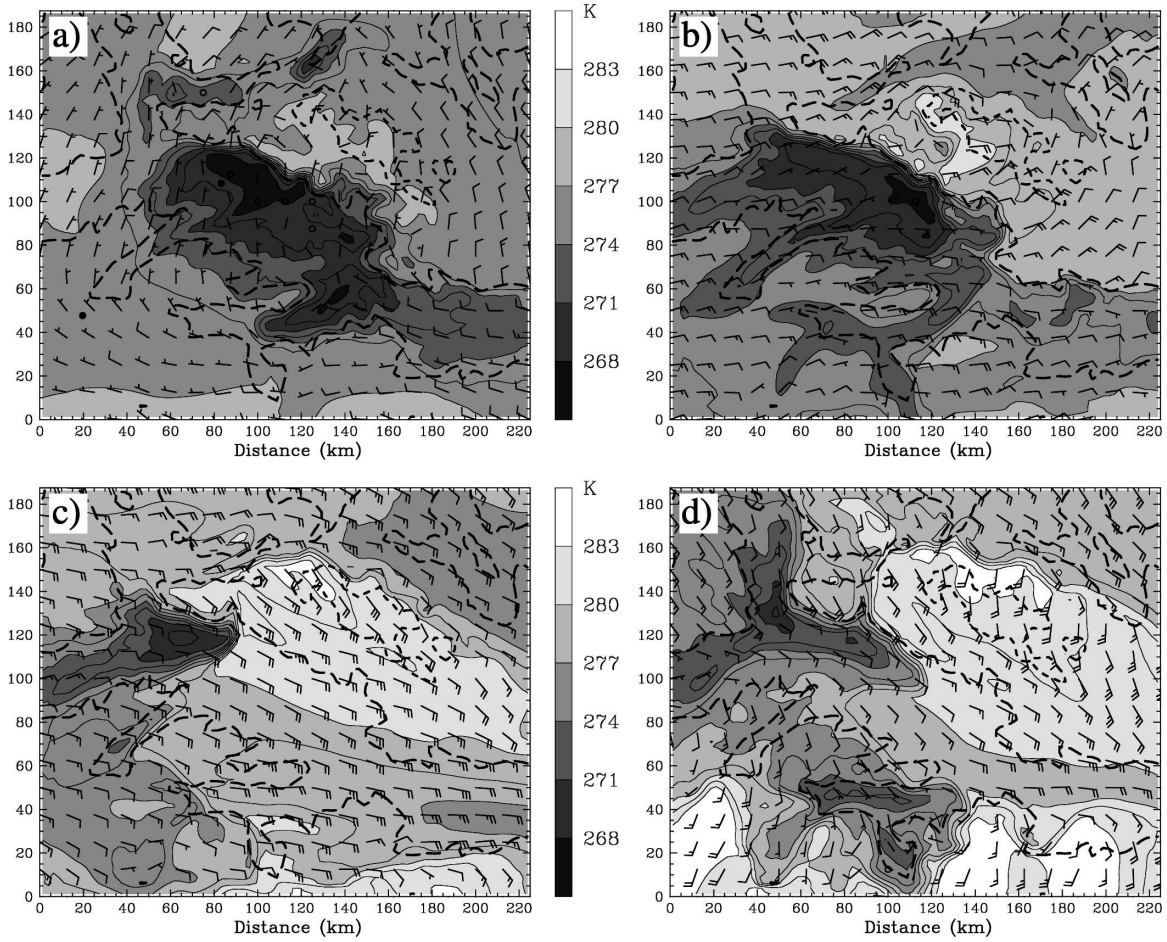

FIG. 4. Surface potential temperature and wind at 85 m AGL for weak-wind simulations with a direction of (a) 45° at $t = 24$ h, (b) 90° at $t = 24$ h, (c) 135° at $t = 18$ h, and (d) 180° at $t = 18$ h. The contour interval (shading increment) is 1.5 (3) K, and a full wind barb corresponds to 5 m s^{-1}. Long (short)-dashed contours indicate a topography height of 450 (900) m as in Fig. 2c. The black dots in (a) indicate the location of Garching and Straubing (see Fig. 2b).

wake. Moreover, the low-level wind speeds are generally higher because the large-scale flow is now roughly parallel to the Alps, reducing the nondimensional height of the Bavarian Forest. This allows the flow to gradually penetrate from the Bavarian Forest into the Danube basin because of gravity wave formation (Fig. 6a). The subsequent flow evolution (not shown) indicates that the warm air reaches the Danube basin both from the Bavarian Forest and from the east, while the cold air is advected downstream. The ageostrophic movement of the cold air toward the lower ambient pressure described by Petkovšek and Vrhovec (1994) and Zängl (2003a) does not seem to be important in this case because the terrain gradually rises toward the south.

The situation drastically changes when a southerly component is added to the ambient wind field. For a direction of 135°, all the cold air is removed from the basin by $t = 21$ h (Fig. 3b), which led us to show the flow field at $t = 18$ h in Fig. 4c. It can be seen that the cold air is advected downstream as well as toward the southwest into the upper Danube Valley, which corresponds to ageostrophic advection. Moreover, the low-level wind speeds are substantially higher than in the previous cases, which obviously enhance the effectiveness of the advection processes. The strong winds arise from flow deflection around the eastern Alps and subsequent channeling into the Danube Valley, which is bounded to the north by an approximately 800-m-high mountain range over a length of about 100 km east of the domain displayed here (see Fig. 2a). As a side effect of the higher wind speeds, pronounced turbulent vertical mixing occurs within the air advected along the Danube Valley, leading to comparatively high surface potential temperatures (see also Fig. 6b).

Southerly ambient flow (Fig. 4d) still induces a strong

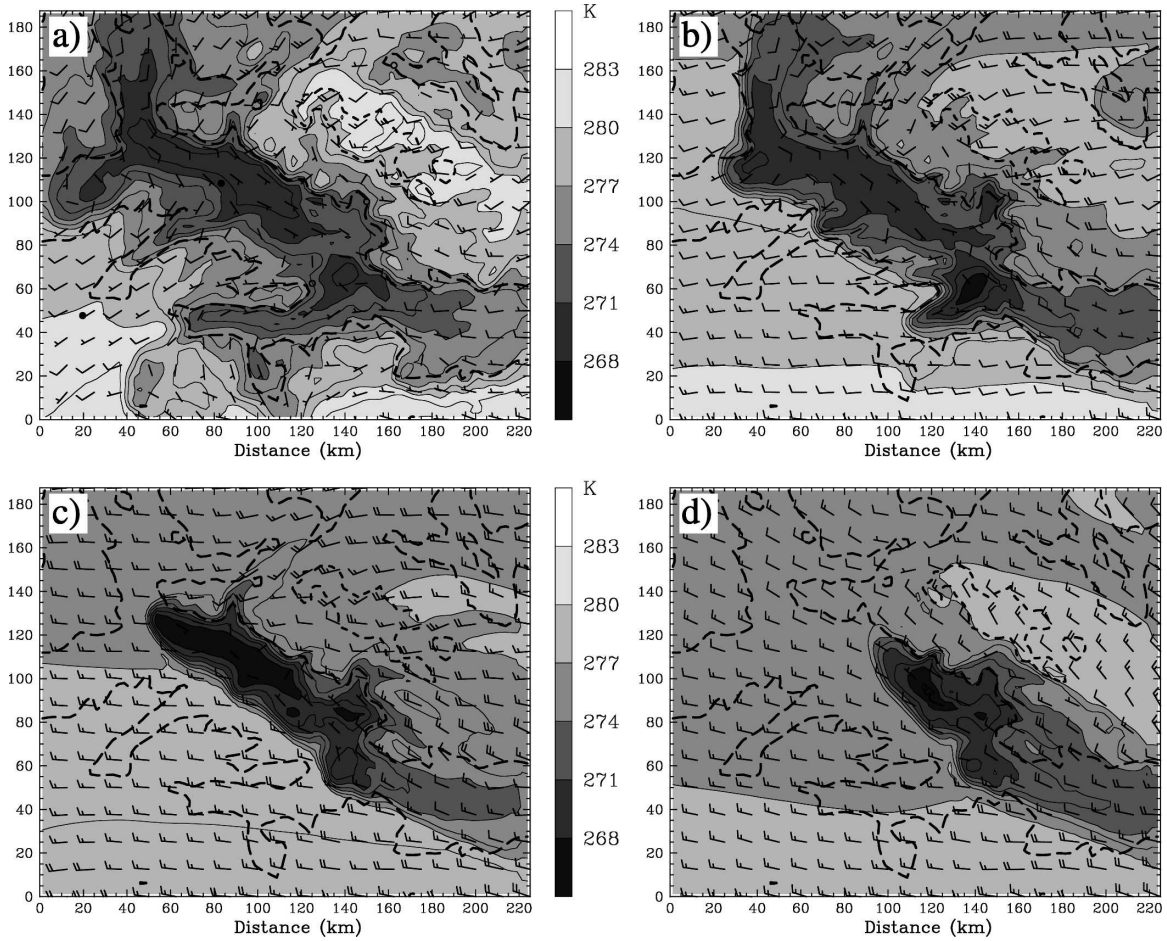

FIG. 5. Same as Fig. 4, but for wind directions of (a) 225° at $t = 24$ h, (b) 270° at $t = 24$ h, (c) 315° at $t = 24$ h, and (d) 360° at $t = 18$ h.

flow deflection around the eastern Alps, yielding a strong easterly low-level flow up the Danube Valley. Consequently, the evolution of the cold pool in the basin area is fairly similar to the 135° case (Fig. 3). Again, the advection of the cold pool out of the basin area is partly downstream and partly ageostrophic. In contrast to the 135° case, potentially very warm air reaches the southern Alpine foreland from the south (foehn), maintaining a substantial temperature difference between Garching and the basin even after the removal of the cold pool proper (Fig. 3e). Moreover, the subsequent evolution of the model fields reveals that the remnants of colder air south of the central part of the Danube basin (Fig. 4d) are dissolved only gradually. This explains why the increase of $\theta_{\min}$ displayed in Figs. 3c,d remains lower for 180° than for 135°.

On the other hand, southwesterly flow favors a fairly high persistence of the cold pool (Fig. 5a). A direct downstream advection of cold air along the large-scale flow direction is prevented by the Bavarian Forest in this case, but there is some deflected downstream advection toward the east. In the majority of the cold pool, the air motion is toward the northwest, corresponding to ageostrophic flow toward the lower ambient pressure. Generally, the wind speeds are fairly low because of the wake effect induced by the Alps, and it will be demonstrated below that the Alpine influence is very important in the 225° case. In the southwestern edge of the domain, there is again evidence of a foehn effect induced by the Alps.

For westerly flow (Fig. 5b), the evolution of the cold pool is quite similar to the southwesterly case, but the wind speed in the southern part of the Alpine foreland is higher because the flow is now parallel to the Alps and therefore not subject to a wake effect. Within the cold pool, ageostrophic motion toward the northwest still dominates over downstream advection, although the former has a pronounced component opposite to the large-scale flow direction. In the literature, a similar phenomenon has frequently been reported for flow

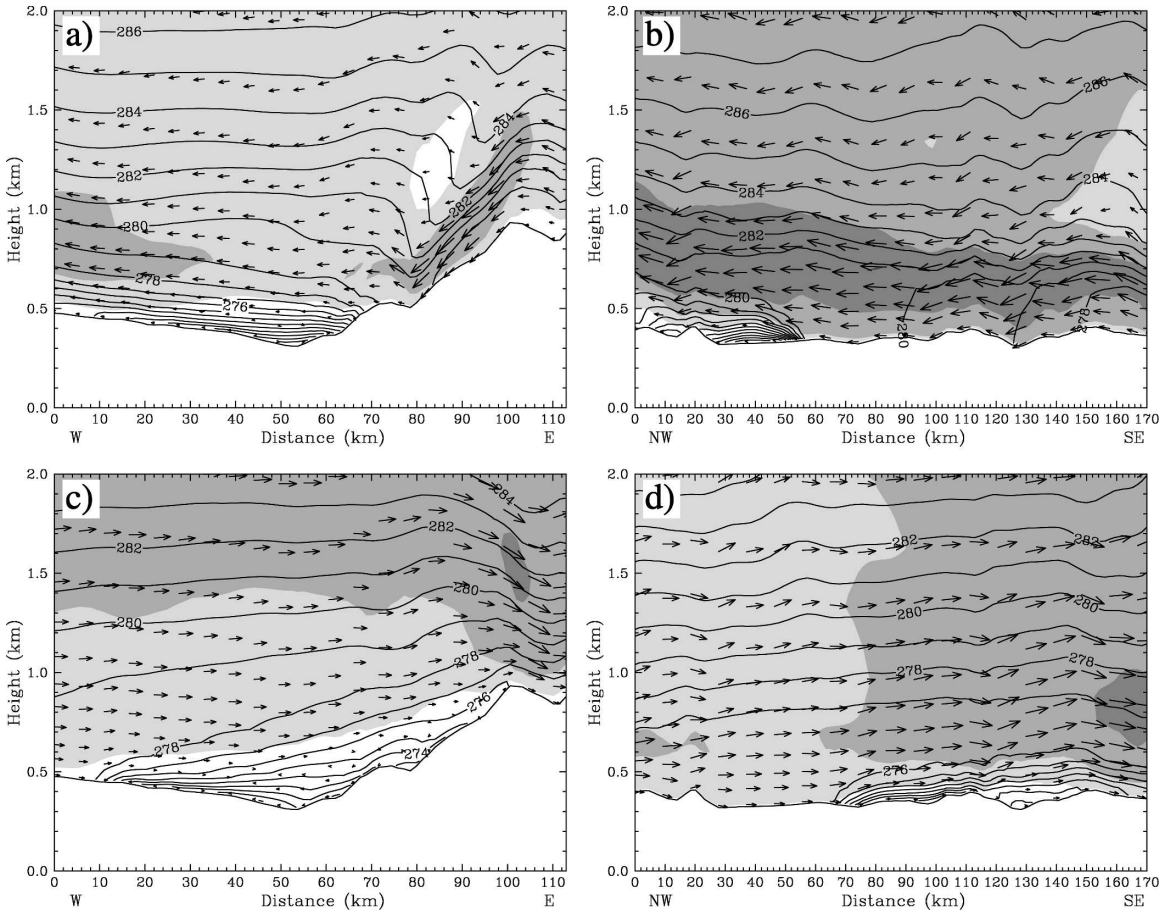

FIG. 6. Vertical cross sections of potential temperature (contour interval 1 K) and cross section–parallel wind component (vectors and shading, shading increment 4 m s^{-1}) along lines (left) a1–a2 and (right) b1–b2. Results are shown for wind directions of (a) 90° at t = 24 h, (b) 135° at t = 18 h, (c) 270° at t = 24 h, and (d) 360° at t = 18 h.

channeling in valleys, even in the absence of a marked cold pool (e.g., Groß and Wippermann 1987; Whiteman and Doran 1993). Here, the ageostrophic motion within the Danube basin is also favored by the upstream flow deceleration induced by the Bavarian Forest. This upstream effect is illustrated in Fig. 6c, showing the cold-air pool piled up on the windward side of the mountain range.

Comparing the westerly and easterly flow cases (Figs. 4b and 5b) reveals that the ageostrophic countercurrent is not present in the easterly case despite a similar orientation of the valley with respect to the flow. This is mainly because the lower Danube Valley (east of the area under consideration) is directed toward the east so that an ageostrophic cold-air outflow would have to continue in a direction exactly opposite to that of the ambient flow. Sensitivity tests without the Bavarian Forest revealed that the upstream–downstream contrast is not essential for this flow feature. Another important difference is found for the surface temperature in the southern part of the Alpine foreland, which is considerably colder for easterly than for westerly flow. This is partly because the air building the initial cold pool is advected toward the Alpine foreland for easterly flow and away from it for westerly flow. However, a more important mechanism is related to the friction-induced ageostrophic wind component near the surface, which is southerly for westerly ambient flow and northerly for easterly ambient flow. As a consequence, there is a tendency for subsidence of potentially warm air in the westerly case while cold air tends to be piled up along the Alpine foothills in the easterly case (see also Zängl 2005b). This also explains the above-mentioned differences between the 90° and 270° cases in Figs. 3c,e. Moreover, the frictional effect on the low-level air modifies the mesoscale pressure field along the Alps (not shown), which further reduces the tendency toward ageostrophic countercurrents in the Danube basin for easterly flow.

The ageostrophic countercurrent in the cold pool dis-

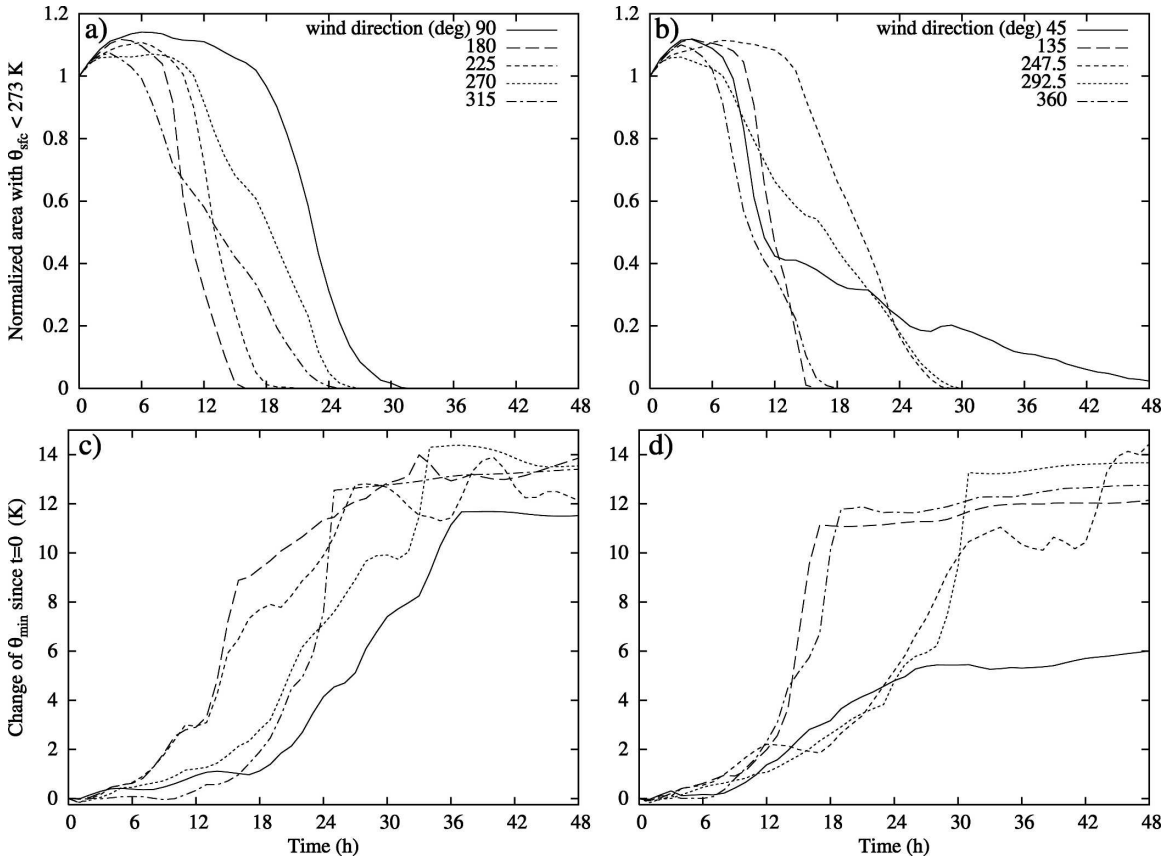

FIG. 7. Same as Figs. 3a–d, but for strong-wind simulations.

appears when adding a northerly component to the westerly flow (292° case, not shown). For this wind direction, the persistence of the cold pool exhibits a weak local maximum (Figs. 3a,b) because the cold-air loss by downstream advection is weaker than in the 315° case (Fig. 5c). Turning the ambient wind to northerly again leads to a very rapid removal of the cold air (Figs. 5d and 6d, results shown for $t = 18$ h) because the low-level flow then becomes roughly parallel to the basin, similar to the 135° case. The removal of the cold air proceeds only somewhat more slowly for 360° than for 135° because the Bavarian Forest prevents a loss of cold air by ageostrophic advection.

b. Strong-wind experiments

All simulations presented in the preceding subsection have been repeated with a steady-state sea level wind speed of 12.5 m s^{-1} (see section 3) in order to check if the results depend qualitatively on the ambient wind speed. Simulations performed with this wind profile will be referred to as strong-wind simulations in the remainder of this paper. The results are summarized in Figs. 7 and 8.

Not surprisingly, increasing the ambient wind speed leads to a faster removal of the cold pool for all wind directions. Except for northeasterly flow, the cold air is completely dissolved within the 48 h of simulation (Fig. 7). However, the flow pattern during this process remains essentially the same in the majority of cases. Specifically, a qualitatively similar evolution has been found for the directions of 247° through 360°, 90°, and 135°, with the exception that the sensitivity to the increased wind speed is weaker for 90° than for the westerly wind directions. This becomes manifest in the fact that in the strong-wind cases, the cold pool takes more time to be dissolved for 90° than for 247° through 315°, while the opposite is the case in the weak-wind series (Figs. 3a,b and 7a,b). The similarity of the flow evolution is illustrated for the 270° case, where the structure of the flow field and of the cold-air pool at $t = 15$ h (Fig. 8a) differs only in minor details from that obtained for the corresponding weak-wind case at $t = 24$ h (Fig. 5b). Note also that the cold pool continues to disappear fastest for wind directions of 135° and 180°, although the difference to the 360° case is smaller than in the weak-wind series.

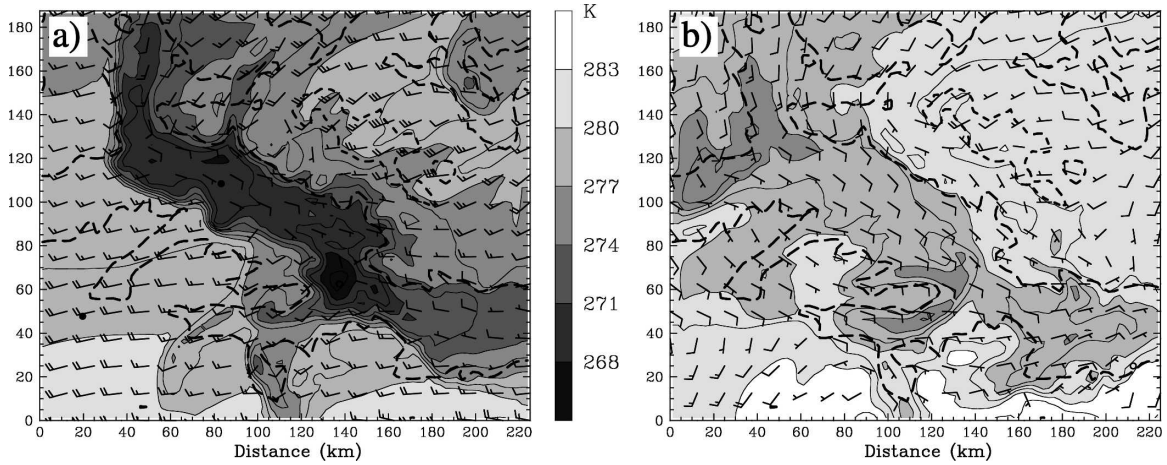

FIG. 8. Same as Fig. 4, but for strong-wind simulations with a direction of (a) 270° at $t = 15$ h and (b) 225° at $t = 24$ h.

Minor structural differences are found for the wind directions of 45° and 180°. At 45°, the cold pool no longer reaches a steady state, although the erosion process advances very slowly. For 180°, the remnants of cold air that were present in the weak-wind case disappear by $t = 30$ h. This has the consequence that the temperature difference between Garching and the coldest point reaches a much smaller value than in the weak-wind case (shown in Fig. 9e below). Moreover, the difference curve no longer exhibits a local extreme around $t = 18$ h because the cold pool is now dissolved before the foehn reaches the grid point of Garching (Fig. 9e).

The most pronounced differences are found for a wind direction of 225°, for which the persistence of the cold pool relative to the other directions greatly decreases (Figs. 3a and 7a). In the strong-wind simulation, the low-level flow deflected around the eastern Alps reaches the Danube basin (Fig. 8b), which is not the case in the weak-wind setting because this flow branch then is not strong enough. Therefore, downstream advection leads to a rapid removal of the cold pool as in the 135° and 180° cases. Nevertheless, a substantial temperature difference between Garching and the basin area is maintained until the end of the simulation because of warm-air subsidence from the Alps (Fig. 9e).

c. Sensitivity tests without Alps

A series of sensitivity experiments has been carried out in order to examine the impact of Alpine flow modification on the persistence of cold-air pools in the Danube basin. In these experiments, the whole Alpine massif is cut at a height of 800 m. The following discussion focuses mainly on downstream effects, because the impact of upstream flow deflection and/or deceleration turned out to be quite weak in most cases. The time series displayed in Fig. 9 show that the persistence of the cold pool generally decreases when the Alps are removed. The largest effect is found for the 225° weak-wind case, followed by the 247° weak-wind case (Figs. 9b,d), and the ordering with respect to the cold-pool persistence gets reversed for these two wind directions. Comparatively small changes occur in the cases in which the cold pool is already rapidly removed in the reference simulations, as is illustrated in Figs. 9a,c for the 180° experiments and the 225° strong-wind case. Generally, the results for the wind directions of 180° and 225° approach each other quite closely without the Alps. For northeasterly flow, the area covered by the cold pool decreases and the minimum temperature increases, but the erosion of the cold pool still proceeds very slowly (Figs. 9b,d). A moderate acceleration of cold-pool erosion is also found in the 45° strong-wind case (not shown). The lower panels of Fig. 9 show that the potential temperature difference between Garching and the Danube basin generally approaches zero without the Alps if the cold pool gets dissolved. This confirms the statement made above that subsidence of potentially warm air from the Alps is responsible for the maintenance of a significant temperature difference in the cases with a southerly flow component.

The flow field during the cold-pool removal process is illustrated in Fig. 10. For the 180° weak-wind case, Fig. 10a confirms that the removal of the cold air has progressed even further after 18 h of simulation than with full topography (Fig. 4d). Moreover, the air mass approaching from the south is very homogeneous because of the flattening of the Alps. Note also that the remnants of cold air in the basin area are located west of the initial cold pool, indicating an ageostrophic

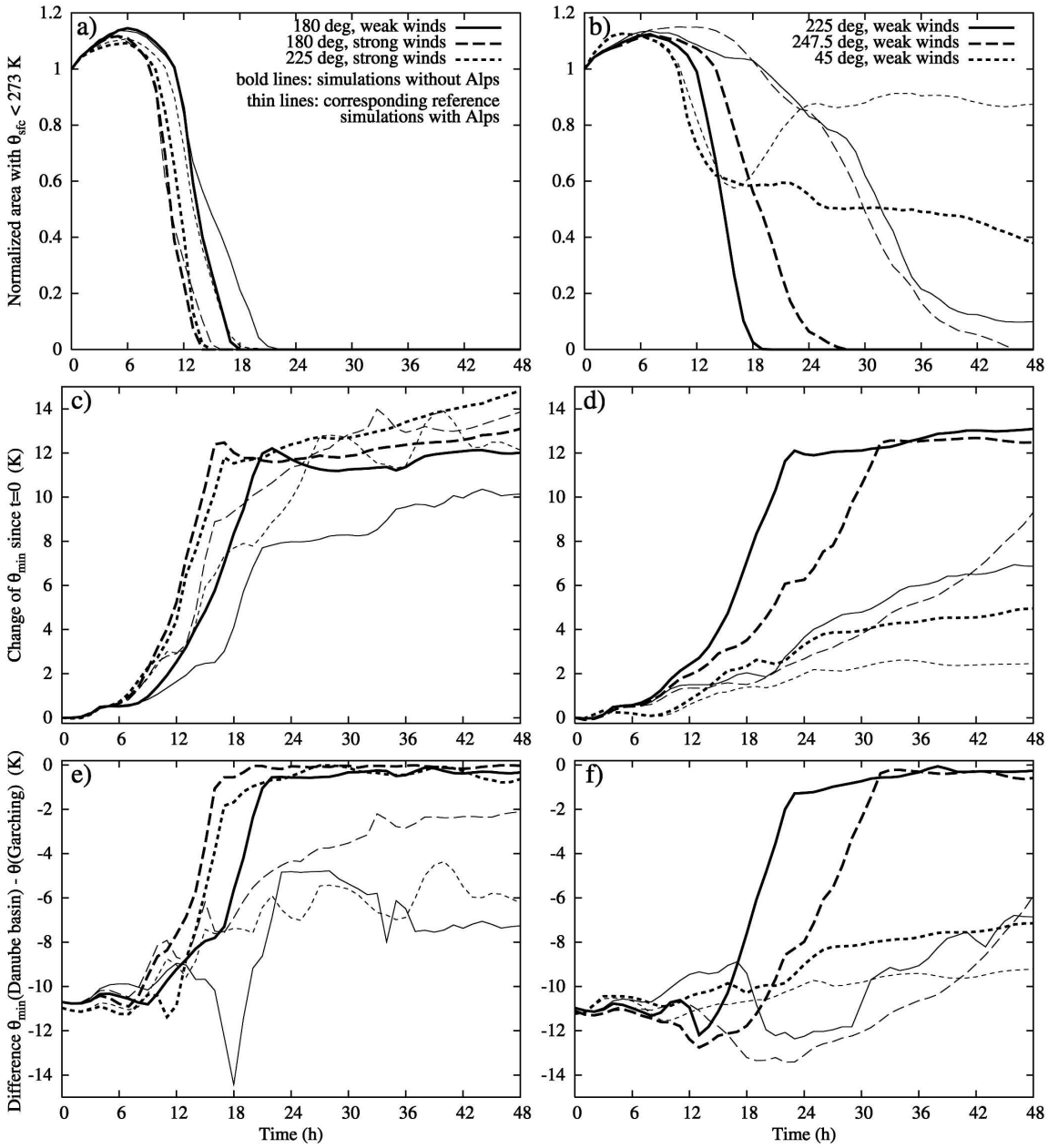

FIG. 9. Same as Fig. 3, but for sensitivity experiments without the Alps. Corresponding reference simulations are displayed with thin lines.

movement of cold air mass toward the lower ambient pressure during the preceding hours. For a direction of 225° (Fig. 10b), ageostrophic motion also dominates within the cold air mass. The vertical cross section along the Danube Valley displayed in Fig. 10d confirms that the southeasterly ageostrophic flow is restricted to the cold pool where the flow is decoupled from the overlying geostrophically balanced flow. The corresponding result for the full-topography run (Fig. 10c) exhibits a much deeper cold-air pool with very little motion because a significant horizontal pressure gradient has not yet been established in this area because of the Alpine wake effect (note that Fig. 5a shows the flow field 6 h later). The large cold-pool depth found in this case, which significantly exceeds that of the initialization (Fig. 2d), results from a combination of subsidence in the lee of the Alps with some piling up of the cold air mass on the windward side of the Bavarian Forest.

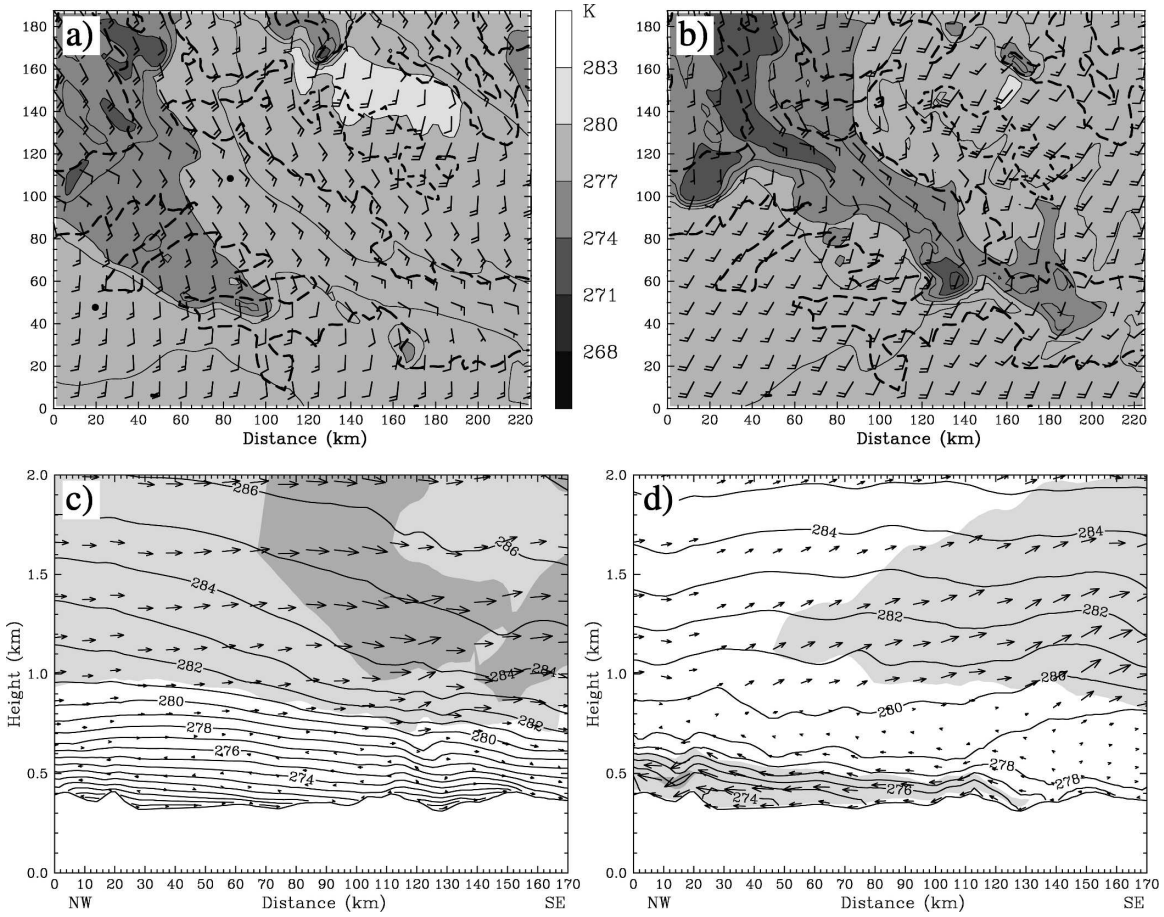

FIG. 10. (top) Same as Fig. 4, but for weak-wind simulations without the Alps and wind directions of (a) 180° at $t = 18$ h and (b) 225° at $t = 18$ h. (bottom) Same as Fig. 6, but for 225° weak-wind simulation (c) with the Alps and (d) without the Alps, at $t = 18$ h. The cross section follows line b1–b2 in Fig. 2b.

Comparing the evolution of the cold-pool area in the no-Alps cases (Figs. 9a,b) with the 270° results displayed in Figs. 3a and 7a, one finds that the cold-pool persistence steadily decreases with an increasing southerly wind component. This is consistent with the idealized results presented by Zängl (2003a) and can be explained by increased ageostrophic advection, which in turn is related to the fact that the projection of the large-scale pressure gradient on the long axis of the basin increases. Relative to the closed elongated basin investigated by Zängl (2003a), the advection efficiency in the along-basin direction is even larger for the realistic topography because the flow does not have to surmount a significant topographic barrier. However, the wake effect of the Alps tends to overcompensate this effect in reality, so that the cold-pool persistence reaches a maximum somewhere between 210° and 260°, depending on the strength of the ambient wind forcing.

d. Sensitivity tests without the Bavarian Forest

The next series of sensitivity tests considers the impact of the Bavarian Forest, the height of which is reduced to 550 m in the following. Results are summarized in Fig. 11. The general tendency found in these experiments in that the presence of the Bavarian Forest improves the persistence of cold-air pools in the Danube basin, but the upstream effect acting under westerly flow conditions turned out to be much less effective that one might expect from Fig. 6c. A significant increase in the longevity of the cold pool resulting from upstream effects was found only for ambient flow directions of 292° (Figs. 11a,c) and 315° (not shown), whereas the 270° experiments showed only a minor impact. In the latter case, the reduced downstream advection resulting from the presence of the Bavarian Forest is counteracted by an increased ageostrophic motion in the along-valley direction, so that the net effect remains

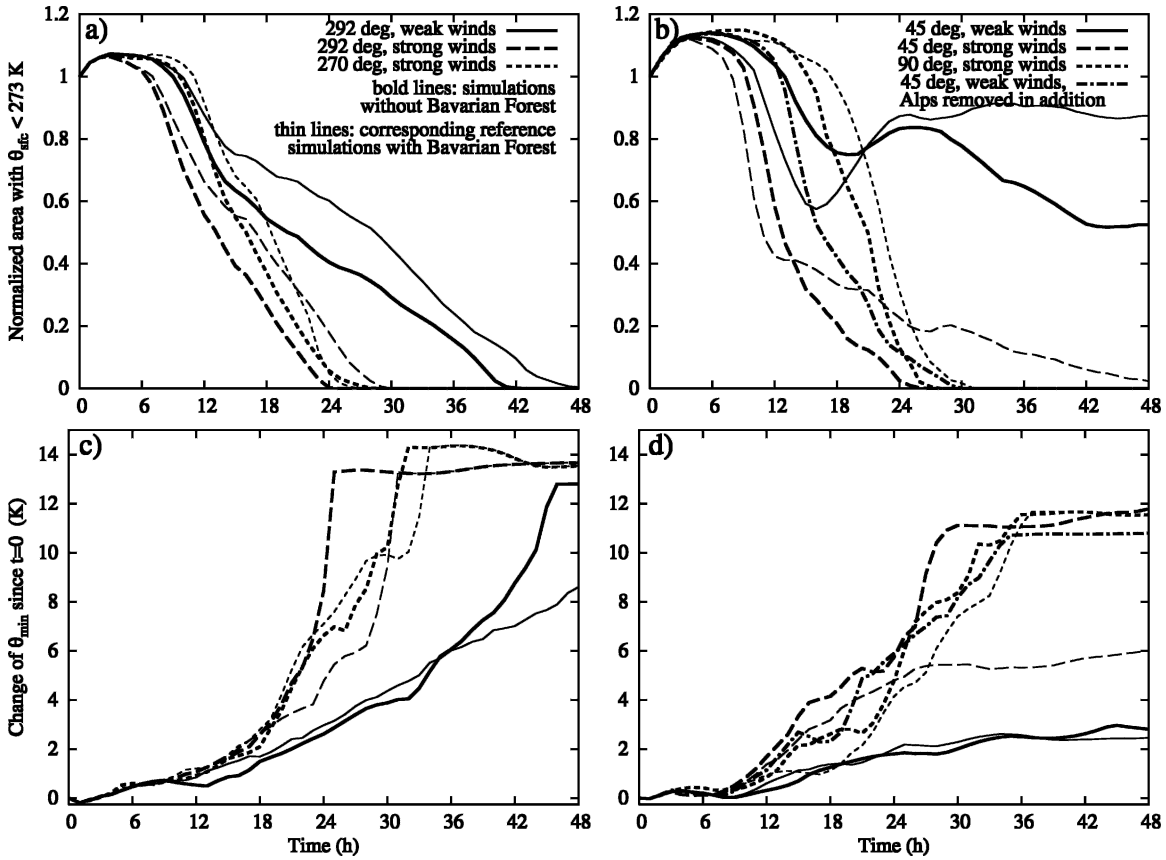

FIG. 11. Same as Figs. 3a–d, but for sensitivity experiments without the Bavarian Forest. Corresponding reference simulations are displayed with thin lines.

small. As demonstrated by Zängl (2003a) for an idealized but structurally similar topography setting, cold-air loss resulting from increased ageostrophic motion can even be the dominating effect of a basin-parallel barrier. For northwesterly large-scale flow, however, the ageostrophic motion within the cold pool is directed toward the Bavarian Forest, so that the presence of the mountain range suppresses the cold-air loss related to this mechanism and therefore enhances the cold-pool persistence.

More complicated behavior was found for the lee effects induced by the Bavarian Forest (Figs. 11b,d). For easterly flow, the wake formation in the lee of the Bavarian Forest slightly increases the persistence of the cold pool, but the impact is not very pronounced (shown for the strong-wind case only). On the other hand, the results for a direction of 45° depend sensitively on the wind speed and on the flow interaction with the Alps. In the weak-wind case with Alps present, cutting the Bavarian Forest again induces only a minor modification, which becomes manifest in a reduced cold-pool area. The minimum temperature in the cold pool remains essentially unchanged. Without the Alps, however, removing the Bavarian Forest greatly decreases the persistence of the cold pool, leading to a temporal evolution similar to that obtained for the 247° case without the Alps (see Fig. 9b). Of course, this major sensitivity might also be attributed to the Alps when presuming the absence of the Bavarian Forest. Taking these results together, one may conclude that the presence of either the Bavarian Forest or the Alps suffices to establish a persistent cold pool in the 45° weak-wind case, while a moderately rapid removal occurs when both topographic barriers are absent. For the Bavarian Forest, this effect can be explained by wake formation, which keeps the winds in the Danube basin very weak. For the Alps, it is related to the fact that the flow-splitting point separating westerly from easterly ridge-parallel flow is quite close to the domain of interest (see also Zängl 2005b). This implies a pronounced reduction of the ambient wind speed, keeping the advective loss of cold air small. Last, in the 45° strong-wind case, the combination of the Bavarian Forest wake and the Alpine upstream effect is needed to es-

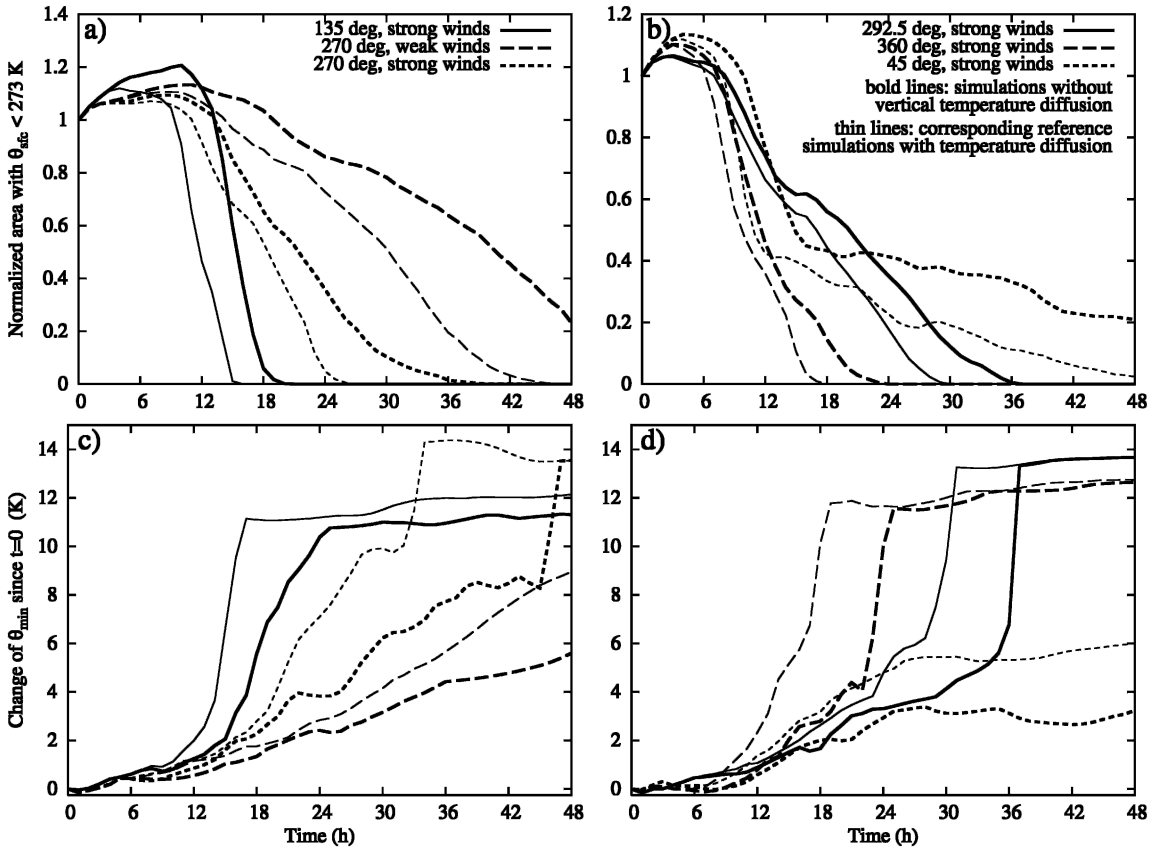

FIG. 12. Same as Figs. 3a–d, but for sensitivity experiments without turbulent vertical mixing. Corresponding reference simulations are displayed with thin lines.

tablish a long-lived cold pool because the Alpine-parallel flow then has an appreciable strength despite the proximity of the flow-splitting point.

e. The impact of turbulent vertical mixing

Most existing studies agree in their conclusion that turbulent vertical mixing usually makes only a minor contribution to the erosion of cold-air pools. However, this conclusion has mostly been based on highly idealized considerations, so that it seems worthwhile reconsidering this issue with dedicated sensitivity tests. Rather than inferring from the presence or absence of TKE that turbulent mixing is likely to have some impact or not, a series of sensitivity tests has been conducted in which the vertical mixing of temperature is explicitly switched off. Recall that this modification is applied in the innermost model domain only, so as to ensure that the stratification of the ambient flow is the same as in the reference experiments, and affects only the mixing of temperature because removing the vertical mixing of momentum would effectively suppress the effects of surface friction.

The results presented in Fig. 12 show that disabling the vertical temperature mixing generally slows down the removal of the cold air. Though being smaller than the spread related to the different wind directions, the impact of temperature mixing is quite appreciable in all cases investigated here. In comparison with idealized considerations, in which vertical mixing is usually assumed to require a local Richardson number below the critical value of 0.25 (e.g., Zhong et al. 2003), this might be partly related to the fact that the mixing schemes commonly used in mesoscale models apply a small background mixing coefficient that is independent of the local TKE value. This background mixing was removed as well in the present sensitivity tests, which might also contribute to the fact that the impact of vertical temperature mixing remains substantial in the weak-wind experiments (Fig. 12a). Another difference to idealized models is that the MM5 accounts for the advection of TKE, so that enhanced mixing is even possible in regions with locally stable conditions. On the other hand, it has to be pointed out that the absence or presence of turbulent mixing does not change the

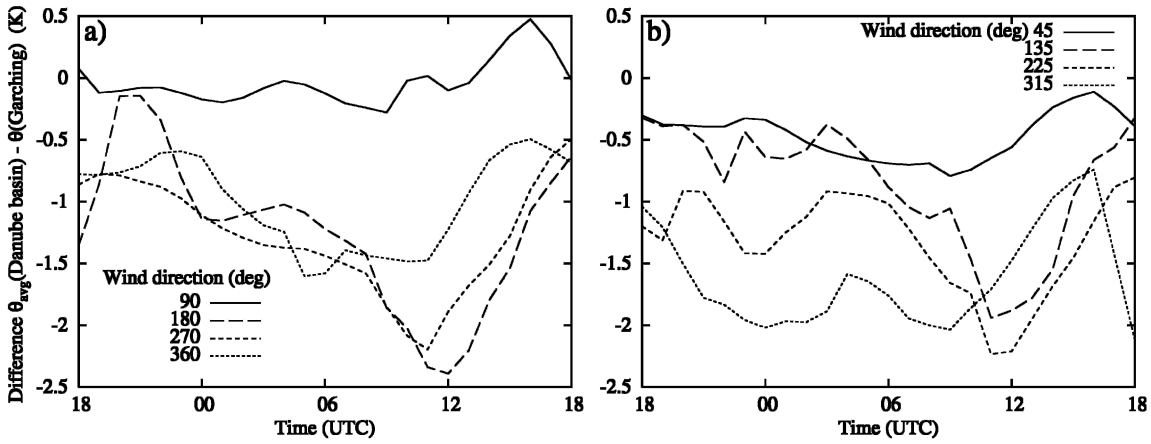

FIG. 13. Model output time series for simulations with radiation, showing the difference between the average surface potential temperature in the central Danube basin and the corresponding value at Garching. The central Danube basin is defined as the area enclosed by the rectangle shown in Fig. 2b and the 400-m isocontour. The time axis is restricted to the second day of simulation.

order of the simulations with respect to cold-pool persistence. Thus, turbulent mixing does not seem to impose an important side effect on the efficiency of the other processes controlling the evolution of a cold pool.

f. Simulations with radiation

Last, a series of experiments has been conducted with radiation in order to examine the dependence of the radiative diurnal temperature cycle on the wind direction. All simulations presented in this subsection use the weak-wind profile and are initialized without a cold pool. Moreover, as already pointed out in section 3, they disregard interactions with fog or stratus clouds. For the second day of the simulation, Fig. 13 depicts the difference between the potential temperature at Garching and the average of the inner Danube basin, defined as the area enclosed by the rectangle shown in Fig. 2b and the 400-m-height isocontour.

Although the spread among the various simulations is much smaller than in the experiments with an initial cold pool, there are some significant qualitative differences to discuss. Most importantly, the potential temperature difference between Garching and the Danube basin is small throughout the day for wind directions of 45° and 90°, while the basin tends to be systematically colder in the other cases. For 135° through 270°, this difference ranges between 0.5 and 1 K at night and between 2 and 2.5 K around noon. An opposite diurnal cycle is found for 315° and 360° with the difference being larger at night than during the day. Thus, the high persistence of cold pools found for 45° and 90° in the previous experiments does not carry over to situations with unimpeded solar radiation. On the other hand, a tendency for colder temperatures in the Danube basin remains present for westerly directions.

The basic mechanism underlying these differences is illustrated in Fig. 14, showing vertical cross sections of potential temperature and wind speed along line c1–a2 in Fig. 2b. For easterly flow, subsidence in the lee of the Bavarian Forest reduces the depth of the nocturnal surface inversion over the Danube basin (Fig. 14a). On the other hand, the friction-induced wind turning in the boundary layer piles up the surface inversion along the northern baseline of the Alps [see Zängl (2005b) for a more thorough discussion of this process], so that the inversion depth in the elevated parts of the Alpine foreland is comparable to that over the basin (Fig. 14a). Consequently, the daytime potential temperature does not tend to be systematically higher in the Alpine foreland than in the Danube basin, and a temperature maximum even appears in the immediate lee of the Bavarian Forest (Fig. 14c). For westerly flow, the situation is reversed. In the Alpine foreland, the nocturnal surface inversion remains shallow because the cold air is constantly advected toward the north by the friction-induced ageostrophic wind component, but the cold air is piled up on the windward side of the Bavarian Forest (Fig. 14b). Thus, the daytime warming over the basin is significantly delayed (Fig. 14d). To complete the interpretation of Fig. 13, we mention that for northwesterly flow, turbulent vertical mixing reduces the nocturnal cooling in the Alpine foreland because a barrier jet forms along the Alps (Zängl 2005b). On the other hand, large-scale lifting on the northern side of the Alps reduces the daytime warming for northerly and northwesterly flow.

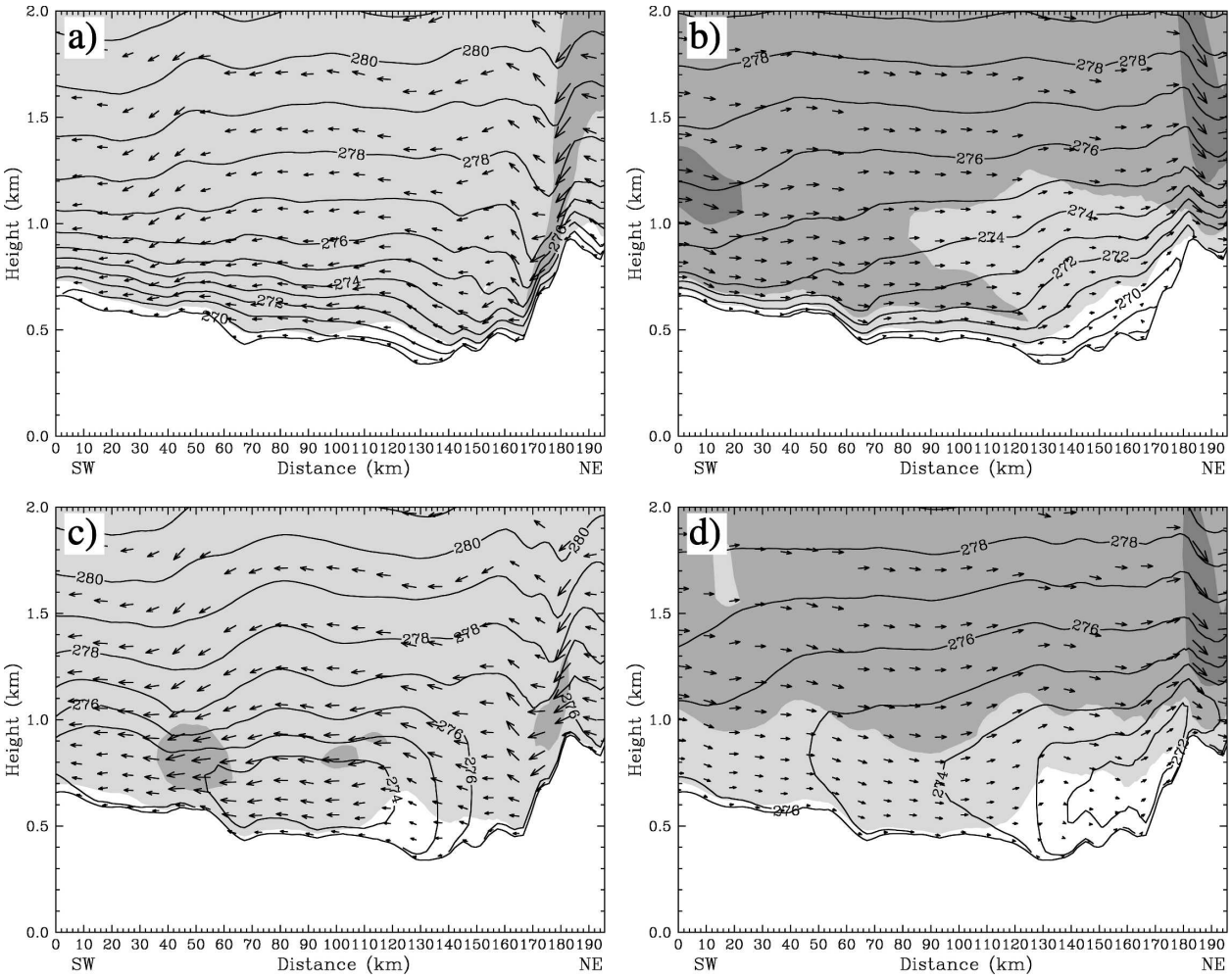

FIG. 14. Vertical cross sections of potential temperature (contour interval 1 K) and cross section–parallel wind component (vectors and shading, shading increment 4 m s^{-1}) along line c1–c2. Results are shown for experiments with radiation and wind directions of (a) 90° at t = 0600 UTC, (b) 270° at t = 0600 UTC, (c) 90° at t = 1200 UTC, and (d) 270° at t = 1200 UTC. All times refer to the second day of the simulation.

5. Discussion

a. Mechanisms affecting the cold-pool evolution

On the basis of the simulations presented in the preceding section, an attempt can be made to compare the importance of the dynamical mechanisms capable of affecting cold-air pools. Obviously, one important mechanism is the ageostrophic advection related to the adjustment of the cold air mass to an external pressure gradient imposed at its top. This mechanism, which has already been investigated for idealized topography configurations by Petkovšek and Vrhovec (1994) and Zängl (2003a), explains the rapid cold-air loss encountered in the no-Alps simulations for wind directions between 180° and 247°. With full topography, however, it is overcompensated by the Alpine wake effect. Note that in the context of channeled flow confined in a valley, the ageostrophic advection is often referred to as "pressure-driven channeling" (e.g., Whiteman and Doran 1993).

A related mechanism, which is not easy to separate from the ageostrophic advection in most cases, is the downstream advection following the ambient wind. In the context of valley winds, this mechanism is usually called "forced channeling." It becomes most relevant when the ambient low-level wind is approximately parallel to the basin or valley, so that the cold air does not need to surmount significant topographic barriers. Possible mechanisms of momentum transfer between the initially stagnant cold pool and the ambient flow are vertical mixing of momentum on top of the cold pool and pressure forces acting at the lateral edges of the

cold pool. The latter mechanism can be expected to be most effective in the presence of a sharp lateral edge such as is shown in Fig. 6b and 6d. Note that for basin-parallel ambient flow, there is still the ageostrophic advection acting perpendicular to the basin, so that the cold-pool persistence is improved by a mountain range on the left-hand side of the basin (looking downstream and assuming positive Coriolis force). For the idealized basin topography studied by Zängl (2003a), the relevance of the downstream advection did not become as evident because the basin was closed at all sides. For realistic topographies, however, this process implies that ambient winds blowing parallel to an elongated basin (or basin-shaped valley) favor a rapid removal of the cold-air pool.

The turbulent vertical mixing of temperature, or at least its representation in MM5, has been found to be of moderate importance in all cases, which does not fully agree with the low relevance ascribed to it in the majority of the previous literature on that topic. However, the similar magnitude of the turbulent mixing in all cases investigated here implies that turbulent mixing is not crucial for understanding the differences among the various wind directions.

Last, an ambivalent picture is found for the up- and downstream effects of surrounding topography. Upstream flow deceleration tends to increase the persistence of cold pools, but flow channeling along a basin-parallel mountain range may reinforce the ageostrophic advection down the ambient pressure gradient so that the net effect may be positive or negative. Likewise, wake formation in the lee of a mountain range tends to improve the maintenance of cold pools at low levels, but subsidence aloft reduces the depth of the cold pool and thus makes it more susceptible to radiative heating, Thus, a snow-covered ground, haze or shallow fog within the basin, or a widespread cloud cover preventing solar heating might be needed to support the maintenance of leeside cold pools.

b. Application to observations

The observational data presented in section 2 indicated a clear warming delay in the Danube basin for all wind directions but easterly, with the correlation between the warming in Munich and the temperature difference between Munich and the basin area being highest for southwesterly to westerly surface winds. For northerly surface winds, the warming delay is small at Regensburg but increases in the down-valley direction. To relate the model results to these observations, it is first necessary to establish the relation between the low-level wind direction at Garching, which entered into the data analysis, and the ambient wind direction specified in the simulations. As can be extracted from Figs. 4 and 5, easterly local winds occur for large-scale directions of 90° and 135°, southerly to southwesterly winds for 180°, southwesterly winds for 225°, westerly winds for 270°–360°, and northwesterly winds for 45°, where the Alpine flow deflection is most pronounced. The complete absence of surface winds from the northerly sector reflects the fact that the Alpine flow deflection prevents a steady northerly flow in the Alpine foreland. In reality, however, northerly surface winds may occur temporarily during frontal passages before the mesoscale flow and pressure field have adjusted to the Alpine barrier effect. Moreover, radiative forcing may induce a diurnal cycle of the surface wind direction with a tendency toward a stronger northerly component during daytime (see e.g., Zängl 2005b), though this effect is presumably small in winter. The low frequency of observed northerly flow (Table 1) corroborates that this wind direction tends to be restricted to comparatively short episodes.

For southwesterly to westerly surface winds, corresponding to large-scale wind directions between 225° and 360°, the simulations consistently indicate a persistent cold pool in the Danube basin except for the 360° case that will be discussed separately below. In addition, subsiding motion from the Alps, related to the friction-induced wind turning or to a general southerly wind component, favors a rapid warming in the southern part of the Alpine foreland (see Figs. 3e,f). Thus, one expects a significant correlation between warming at Munich or Garching and a temperature deficit in the Danube basin, in accordance with the data analysis. For southerly flow, the simulations indicate a comparatively rapid warming in the Danube basin, but nevertheless, a substantial temperature difference is maintained between Munich and the basin region resulting from subsidence of potentially warm air from the Alps. Thus, we again expect a temperature increase in Munich to coincide with lower temperatures in the basin area.

For easterly surface wind, corresponding to large-scale wind directions between 90° and 135°, a different picture arises. According to the model results, southeasterly flow tends to rapidly remove the cold air in the Danube basin, so that no significant warming delay relative to the region of Munich is expected. For easterly large-scale flow, the model predicts a long-lived cold pool in the Danube basin, but the cold pool is shallow resulting from subsidence aloft and therefore is sensitive to radiative heating. Moreover, when assuming that the initial cold air is not restricted to the basin area, advective warming in the southern part of the Alpine foreland will proceed much more slowly than for westerly directions because the friction-induced

northerly wind component tends to pile up the cold air along the Alpine foothills (see also Fig. 3e, where the initial temperature difference decreases faster than $T_{\min}$ increases because of cooling at Garching). It also has to be mentioned that advective warming is less likely for easterly flow than for southeasterly flow in the winter months because the land–sea contrast favors cold air in the east. This is even more so the case for northeasterly flow, which therefore should be disregarded in this context.

For a large-scale wind direction around 360° a frontal passage would probably be associated with temporary northerly surface winds, although the simulated flow field indicates westerly wind at Garching. Therefore, this case should be compared with northerly observed flow (330°–60°), for which Table 1 indicates a small warming delay at Regensburg, a moderate delay at Straubing, and a substantial delay at Passau. This pattern is consistent with the downstream advection of the cold pool obtained in the 360° run (Fig. 5d), which implies that the warming progresses from northwest to southeast. It should be noted, however, that warm-air advection from the north is also very unlikely, except perhaps when air of subtropical origin is deflected around a high over western Europe.

6. Conclusions

In this study, idealized numerical simulations have been presented in order to investigate the characteristics of cold-air pools in the Bavarian Danube basin. They are initialized with a pronounced cold pool in the basin area and examine the response of the cold pool to the dynamical forcing imposed by a geostrophically balanced large-scale wind field of various directions and strengths. The simulations are used to explain the observational evidence that the warming delay in the basin region with respect to the more elevated parts of the Alpine foreland depends sensitively on the large-scale wind direction. In addition, sensitivity experiments were conducted in which the major topographic features specific to this region (Alps and Bavarian Forest) are removed. Apart from revealing the dynamical impact of these mountain ranges on cold-air pools in the Danube basin, these experiments will also facilitate a future application of the present results to other basin regions of the world. Further sensitivity tests considered the impact of vertical temperature mixing and radiation.

According to the model results, the main dynamical processes controlling the evolution of cold-air pools in a large basin are the adjustment to an external pressure gradient imposed on top of the cold pool, leading to ageostrophic advection of the cold air toward the lower ambient pressure, and downstream advection by the ambient flow. Both advection processes are most efficient along directions where the surrounding topography is low, which is usually the along-basin direction when the basin is related to a river valley. Turbulent vertical mixing also makes a significant contribution to the erosion of cold pools, but its effect seems to be quite independent of wind direction. Thus, turbulent mixing is not crucial for the dependence of the cold-pool persistence on the ambient wind direction. However, upstream effects as well as lee effects of surrounding topography have the potential to significantly affect the dynamics of cold-air pools, depending on the actual topography configuration. For the specific case of the Danube basin, the Alps substantially enhance cold-pool persistence resulting from wake effects under southwesterly flow conditions, and slightly enhance cold-pool persistence under northeasterly flow conditions because of upstream blocking effects. The Bavarian Forest counteracts the ageostrophic advection for northwesterly flow and induces a wake effect for easterly and northeasterly flow, but the latter is associated with subsidence aloft so that the cold pool gets more susceptible to radiative forcing because it is reduced in depth. Taking all of these effects together, the model predicts a higher persistence of the cold pool for westerly and southwesterly flow than for easterly flow, which is consistent with the observational data.

A future extension of this work could examine the interaction of radiation with cold-air pools in more detail, particularly in the presence of fog/haze or a snow cover. As indicated by the present simulations, at least one of these factors is needed to obtain a persistent cold-air pool in a shallow basin unless the radiation is generally weak because of widespread cloud cover. Moreover, experiments with directional wind shear or passing fronts could be conducted as a further step toward reality.

Acknowledgments. The author expresses his gratitude to the German Weather Service (DWD) for providing the observational data analyzed in this study.

REFERENCES

Colette, A., F. K. Chow, and R. L. Street, 2003: A numerical study of inversion-layer breakup and the effects of topographic shading in idealized valleys. *J. Appl. Meteor.,* **42,** 1255–1272.

Dudhia, J., 1989: Numerical study of convection observed during the Winter Monsoon Experiment using a mesoscale two-dimensional model. *J. Atmos. Sci.,* **46,** 3077–3107.

Fast, J. D., S. Zhong, and C. D. Whiteman, 1996: Boundary layer evolution within a canyonland basin. Part II: Numerical simulations of nocturnal flows and heat budgets. *J. Appl. Meteor.,* **35,** 2162–2178.

Grell, G. A., J. Dudhia, and D. R. Stauffer, 1995: A description of

the fifth-generation Penn State/NCAR Mesoscale Model (MM5). NCAR Tech. Note NCAR/TN-398+STR, 122 pp.

Groß, G., and F. Wippermann, 1987: Channeling and countercurrent in the upper Rhine Valley: Numerical simulations. *J. Climate Appl. Meteor.,* **26,** 1293–1304.

Klemp, J. B., and D. R. Durran, 1983: An upper boundary condition permitting internal gravity wave radiation in numerical mesoscale models. *Mon. Wea. Rev.,* **111,** 430–444.

Lee, T. J., R. A. Pielke, R. C. Kessler, and J. Weaver, 1989: Influence of cold pools downstream of mountain barriers on downslope winds and flushing. *Mon. Wea. Rev.,* **117,** 2041–2058.

Mlawer, E. J., S. J. Taubman, P. D. Brown, M. J. Iacono, and S. A. Clough, 1997: Radiative transfer for inhomogeneous atmosphere: RRTM, a validated correlated-k model for the longwave. *J. Geophys. Res.,* **102,** 16 663–16 682.

Petkovšek, Z., 1985: Die Beendigung von Luftverunreinigungsperioden in Talbecken (The termination of air pollution periods in basins). *Z. Meteor.,* **35,** 370–372.

——, 1992: Turbulent dissipation of cold air lake in a basin. *Meteor. Atmos. Phys.,* **47,** 237–245.

——, and T. Vrhovec, 1994: Note on influences of inclined fog lakes on the air pollution in them and on the irradiance above them. *Meteor. Z.,* **3,** 227–232.

Rakovec, J., J. Merše, S. Jernej, and B. Paradiž, 2002: Turbulent dissipation of the cold-air pool in a basin: Comparison of observed and simulated development. *Meteor. Atmos. Phys.,* **79,** 195–213.

Schär, C., D. Leuenberger, O. Fuhrer, D. Lüthi, and C. Girard, 2002: A new terrain-following vertical coordinate for atmospheric prediction models. *Mon. Wea. Rev.,* **130,** 2459–2480.

Schipper, J. W., 2005: Downscaling of precipitation in the upper Danube catchment area. Ph.D. thesis, University of Munich, 92 pp.

Shafran, P. C., N. L. Seaman, and G. A. Gayno, 2000: Evaluation of numerical predictions of boundary layer structure during the Lake Michigan Ozone Study (LMOS). *J. Appl. Meteor.,* **39,** 412–426.

Vrhovec, T., 1991: A cold air lake formation in a basin—A simulation with a mesoscale numerical model. *Meteor. Atmos. Phys.,* **8,** 91–99.

——, and A. Hrabar, 1996: Numerical simulations of dissipation of dry temperature inversions in basins. *Geofizika,* **13,** 81–96.

Whiteman, C. D., 1982: Breakup of temperature inversions in deep mountain valleys: Part I. Observations. *J. Appl. Meteor.,* **21,** 270–289.

——, and T. B. McKee, 1982: Breakup of temperature inversions in deep mountain valleys: Part II. Thermodynamic model. *J. Appl. Meteor.,* **21,** 290–302.

——, and J. C. Doran, 1993: The relationship between overlying synoptic-scale flows and winds within a valley. *J. Appl. Meteor.,* **32,** 1669–1682.

——, S. Zhong, and X. Bian, 1999a: Wintertime boundary layer structure in the Grand Canyon. *J. Appl. Meteor.,* **38,** 1084–1102.

——, X. Bian, and S. Zhong, 1999b: Wintertime evolution of the temperature inversion in the Colorado Plateau basin. *J. Appl. Meteor.,* **38,** 1103–1117.

Zängl, G., 2002a: Stratified flow over a mountain with a gap. Linear theory and numerical simulations. *Quart. J. Roy. Meteor. Soc.,* **128,** 927–949.

——, 2002b: An improved method for computing horizontal diffusion in a sigma-coordinate model and its application to simulations over mountainous topography. *Mon. Wea. Rev.,* **130,** 1423–1432.

——, 2003a: The impact of upstream blocking, drainage flow and the geostrophic pressure gradient on the persistence of cold air pools. *Quart. J. Roy. Meteor. Soc.,* **129,** 117–137.

——, 2003b: A generalized sigma coordinate system for the MM5. *Mon. Wea. Rev.,* **131,** 2875–2884.

——, 2005a: Dynamical aspects of wintertime cold-air pools in an Alpine valley system. *Mon. Wea. Rev.,* **133,** 2721–2740.

——, 2005b: Large-scale-flow interactions with the Alps and their impact on the low-level temperature field in the northern foreland. *Meteor. Z.,* **13,** 379–386.

Zhong, S., C. D. Whiteman, X. Bian, W. J. Shaw, and J. M. Hubbe, 2001: Meteorological processes affecting the evolution of a wintertime cold air pool in the Columbia basin. *Mon. Wea. Rev.,* **129,** 2600–2613.

——, X. Bian, and C. D. Whiteman, 2003: Time-scale for cold-air pool breakup by turbulent erosion. *Meteor. Z.,* **12,** 229–233.